RapidAIM: A culture- and metaproteomics-based Rapid Assay of Individual Microbiome responses to drugs

Leyuan Li[1], Zhibin Ning[1], Xu Zhang[1], Janice Mayne[1], Kai Cheng[1], Alain Stintzi*[1], Daniel Figeys*[1,2,3]

[1] Department of Biochemistry, Microbiology and Immunology, Ottawa Institute of Systems Biology, Faculty of Medicine, University of Ottawa, Ottawa, Canada

[2] Department of Chemistry and Biomolecular Sciences, University of Ottawa, Ottawa, Canada

[3] Canadian Institute for Advanced Research, Toronto, Canada

* Corresponding Authors, Email: dfigeys@uottawa.ca (DF), and astintzi@uottawa.ca (AS)

Abstract

The gut microbiome has been associated with a growing list of diseases. Drugs and other compounds can affect the microbiome, but our understanding of drug-induced changes in individual microbiomes is limited due to a lack of rapid and effective high-throughput assay methods. We developed an approach named Rapid Assay of Individual Microbiome (RapidAIM) to screen xenobiotics against individual microbiomes. RapidAIM was evaluated by testing 43 compounds against five individual microbiomes using a metaproteomic approach. We show that our workflow enables quantitative profiling of the microbiome. The tested compounds significantly affected overall microbiome abundance, microbiome composition and functional pathways at multiple taxonomic levels. The microbiome responses to berberine, metformin, diclofenac, fructooligosaccharide and most antibiotics were consistent among most individuals. Interestingly, most of our tested NSAIDs, statins, and histamine-2 blockers induced strong and individually distinct responses. Our workflow offers an effective solution to systematically study the effects of many different compounds on individual microbiomes.

Main

The gut microbiome has been linked to gastroenterological, neurologic, respiratory, metabolic, hepatic, and cardiovascular diseases[1]. Targeting the microbiome could lead to novel therapies[2].

Although the effects of some drugs and compounds on the microbiome have been reported[3], many drug-microbiome interactions are unknown. This is due in part to the extremely high numbers of marketed drugs[4] and compounds in development[5] together with the lack of assays that can rapidly assess the effects of compounds on individual microbiomes.

Different *in vitro* strategies have been employed to study drug-microbiome interactions. One strategy involves long term stabilization of the microbiome, as shown in various intestinal microbiome simulators based on continuous flow[6-8]. This approach typically requires a long culture period to stabilize the microbiome (15-20 days), and notable shifts in taxonomic compositions compared with the inoculum have been shown[9,10]. Moreover, the size and complexity of these culturing systems limit the number of individual microbiomes and drugs that can be examined[8]. Another strategy is to culture individual bacteria strains isolated from microbiomes. A recent study examined the effects of over 1,000 drugs on the biomass of 40 individually-cultured bacterial strains[11]. Although this approach may identify novel antibacterial effects, it does not take into account bacteria-bacteria interaction and the complex environment of a microbial community; for example, bacteria living in biofilms can resist antibiotics that would kill individual bacteria cells[12]. Thus, it is important to study drug effects in the context of a microbial community.

The development of meta-omics approaches has allowed rapid and deep measurement of microbiome compositions and functional activities. 16S rDNA gene sequencing has the advantages of high-throughput and a relatively inexpensive cost[13]. However, 16S rDNA analyses suffer from limited taxonomic resolution. Shotgun metagenomics enables deeper taxonomic resolution and provides information about the microbiome functional capability[13,14]. However, metagenomics offers little insight on which microbial traits actually contribute to the functional activities of the studied microbiome, as genes predicted from metagenomics analyses are not necessarily expressed. For this reason, the metaproteome, and to some extent the metatranscriptome, better reflect microbial functions. More specifically, mass spectrometry (MS)-based metaproteomics technology provides in-depth insight into microbiome function[15,16]. In addition to precisely quantifying microbial functional activities, MS-based metaproteomics can accurately quantify taxon-specific biomass contributions[17]. However, despite its great potential in analyzing microbiome responses to drugs, current metaproteomics approaches have

not been adapted for a high-throughput workflow that enables the comparisons of biomass, composition and function between different microbiomes.

Given the above, there's a lack of an *in vitro* assay that studies the drug responses of a gut microbiome ecosystem in a high-throughput manner, and that can provide comprehensive biomass, compositional and functional information using a single analytical tool.

Here we report an approach named Rapid Assay of an Individual's Microbiome (RapidAIM). Briefly, in RapidAIM, individual microbiomes are cultured in 96-well plates for 24 hours and the effects of drugs on the microbiome composition and function are studied with various omics approaches. In this study, we use a metaproteomics-based analytical approach to gain functional insight into the individual microbiomes responses following drug treatments.

Results

Development and evaluation of RapidAIM

RapidAIM consists of an optimized microbiome culturing method that enables the study of microbial-drug interactions. In this study, RapidAIM is coupled with an equal-volume based protein extraction and digestion workflow and a metaproteomic analysis pipeline **(Figure 1a)**. Briefly, fresh human stool samples are inoculated in 96-well deep-well plates and cultured with drugs for 24 hours. We have previously optimized the culture conditions that maintain the composition and taxon-specific functional activities of individual gut microbiomes in 96-well deep-well plates (paper under review). After 24 hours, the microbiomes in the 96-well plate are prepared for metaproteomic analysis **(Supplementary Figure S1)** using a microplate-based metaproteomic sample processing workflow **(Supplementary Figure S1)** adapted from our single-tube protocol[18]. The microplate-based workflow consists of: bacterial cell purification, cell lysis under ultra-sonication in 8M urea buffer, in-solution tryptic digestion, and desalting. We validated each step of this workflow and found no significant differences in identification efficiency between 96-well plate processing and single-tube processing **(Supplementary Figure S1)**.

Finally, the microbiomes from each well are analyzed by metaproteomics[19-21]. To compare total biomass, taxon-specific biomass and pathway contributions between samples in a high-throughput assay format, we applied an equal sample volume strategy to our recently developed

metaproteomics techniques[19-21]. First, to validate the relative quantification of total bacterial biomass by comparing total peptide intensity, an equal volume of samples from a microbiome dilution series (simulating different levels of drug effects) was taken for tryptic digestion and LC-MS/MS analysis. Summed peptide intensity in each sample showed good linearity (R^2 = 0.991, **Figure 1b**) with a standard colorimetric protein assay, showing that the total peptide intensity is a good indicator for microbiome biomass levels. We then evaluated whether biomass differences between wells could cause identification bias. We confirmed that the level of total biomass didn't bias data quantifications, including functional profiles (**Figure 1c**), protein group quantifications (**Supplementary Figure S2a**), and taxonomic biomass contributions[17] (**Supplementary Figure S2b**).

RapidAIM: Proof-of-concept study

We conducted a proof-of-concept (POC) study on the use of RapidAIM to characterize drug-microbiome interactions. We selected 43 compounds that have been previously shown to impact or interact with the gut microbiome (**Supplementary Table S1)**. Thirty-seven of these compounds are FDA-approved drugs; four are antibiotics, and the others include NSAIDs, anti-diabetic drugs, aminosalicylate, and statins. Each compound, at a dose corresponding to the assumed maximal fecal concentration of its daily dose, was added to five wells of 96-well plates containing 1 ml culture medium in each well. The drug solvent, DMSO, was used as the negative control. Then, each of the five wells for each compound was inoculated with a different fecal microbiome from healthy human volunteers, generating a $(43 + 1) \times 5$ matrix. Following 24 hours of culturing, the 220 samples were processed through the microplate-based workflow **(Figure S1)** and were subjected to a 90 min gradient-based rapid LC-MS/MS analysis. Using our automated metaproteomic data analysis software MetaLab[20], 101,995 peptide sequences corresponding to 24,632 protein groups were quantified across all samples with a false discovery rate (FDR) threshold of 1% **(Figure 1e)**. The average MS/MS identification rate was 32.4 ± 8.8% (mean ± SD); an average of 15,017 ± 3,654 unique peptides and 6,684 ± 998 protein groups were identified per sample. To provide a global analysis of the microbiome responses, a PCA was performed based on LFQ intensities of protein groups **(Figure 1f)**. As expected, the samples clustered based on the original microbiome source and not based on drug treatment.

Within each individual microbiome group, a number of drug-treated samples clustered closely to their control while several drug-treated samples clearly separated from the non-treated control.

We next evaluated the robustness and reproducibility of the method by culturing one microbiome with drugs in technical triplicates. Cultured triplicates yielded high Pearson's *r* for LFQ protein group intensities **(Figure 1d**). Hierarchical clustering based on Pearson's *r* of LFQ protein group intensities between samples showed that with the exception of several compounds which clustered closely with DMSO, cultured triplicates were clustered together **(Supplementary Figure S3a)**. Moreover, total biomass, functional enzymes, and species biomass contributions were highly reproducible between triplicates as shown in **Supplementary Figure S3b-d**.

Finally, we assessed whether RapidAIM recapitulates known *in vivo* microbiome responses to drugs. *In vitro* microbiome responses were consistent with several existing *in vivo* studies[22-29], including FOS, indomethacin, isoniazid, berberine and metformin effects on the gut microbiome **(Supplementary Figure S4)**.

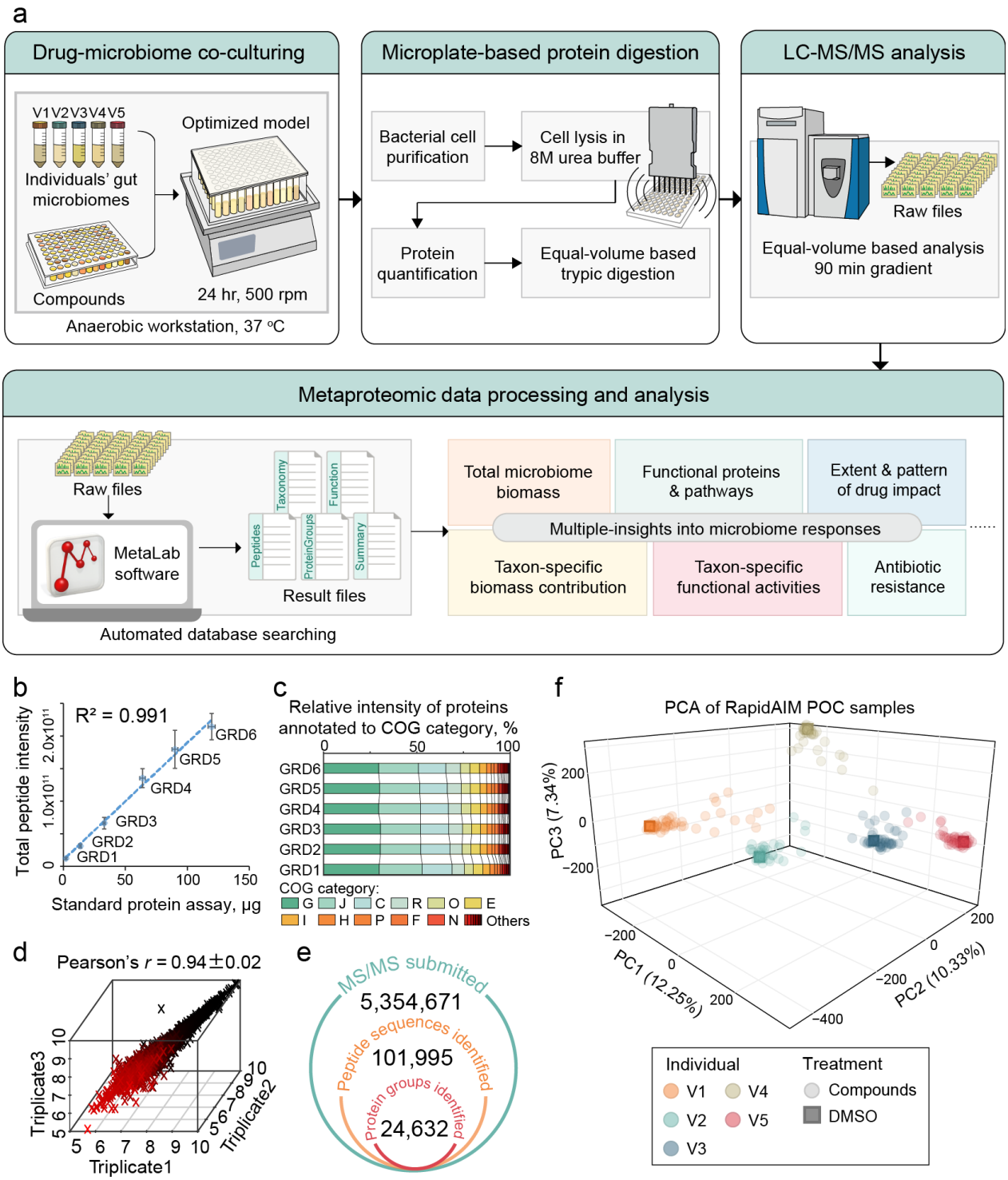

Figure 1. Rapid Assay of Individual Microbiome (RapidAIM) workflow and performance. (**a**) Experimental, analytical, and bioinformatics components of the RapidAIM workflow. Each individual's gut microbiome samples are cultured with the test compounds in a 96-well deep-well plate at 37℃ in strict anaerobic conditions for 24 hours followed by high-throughput sample

preparation and rapid LC-MS/MS analysis. Peptide and protein identification and quantification, taxonomic profiling, and functional annotation were performed using the automated MetaLab software[20]. (**b**) A series of six dilutions (dilution gradients: GRD1~6) of a same microbiome sample was tested in triplicate through the equal-volume digestion and equal-volume MS loading protocol; the summed peptide intensity was compared to a set of protein concentration standards provided with DC protein concentration assay and showed good linearity (center points and error bars represent mean ± SD). (**c**) Stacked bars of clusters of orthologous groups (COG) category levels across the six concentrations showing no bias at the functional quantifications. (**d**) Analysis of three technical replicates in RapidAIM showing high Pearson's correlation. (**e**) Numbers of MS/MS submitted, peptide sequence and protein group identifications in the proof-of-concept (POC) dataset. (**f**) PCA based on LFQ intensities of protein groups for all POC samples.

Effects of compounds on microbiome abundance and composition

We examined the effect of the 43 compounds on the overall abundance (biomass) of each individual microbiome by comparing the total peptide intensity **(Figure 2a)**. As expected, the antibiotics rifaximin, ciprofloxacin and metronidazole greatly reduced total microbial biomass in most individual microbiomes. Berberine, ibuprofen, isoniazid, diclofenac and indomethacin also mildly inhibited the biomass of all individual microbiomes.

We next explored the effects of drugs on the microbiome composition. We first took a brief view by visualizing the responses of the 20 most abundant genera across all samples (**Figure 2b**). As expected, the broad-spectrum antibiotics rifaximin, ciprofloxacin and metronidazole decreased the absolute abundance of these bacterial genera. In addition, **Figure 2b** shows that *Bifidobacterium* was increased by FOS in all samples, and 3/5 samples showed an increase in *Akkermansia* in response to berberine. *Gordonibacter* was decreased in response to FOS, isoniazid and mercaptopurine in most microbiomes.

To evaluate the overall shift of the microbiome, Bray-Curtis distance[30,31] between drug-treated and DMSO control microbiome indicated that FOS, rifaximin, berberine, diclofenac, ciprofloxacin, metronidazole and isoniazid significantly shifted the microbiome (pairwise Wilcoxon test, FDR-adjusted $p < 0.05$; **Figure 2c**).

In addition to the overall shifts in microbiome composition, we examined the biomass of individual bacterial species in the microbiomes. We found that 36 of the 43 compounds

significantly affected the biomass of at least one bacterial species (one-sided Wilcoxon rank sum test, FDR-adjusted $p < 0.05$; **Supplementary Table S2**). We then compared the bacterial response we observed in microbiome cultures to the response reported in a previous study of isolated bacterial cultures[11]. Besides the antibiotics, six of the compounds we tested (methotrexate, azathioprine, mercaptopurine, simvastatin, flucytosine, and digoxin) were previously shown to have antibiotic-like effects on isolated bacterial strains[11]. In response to these six compounds, our microbiome-based assay suggested four significant inhibitions which were also found in the isolated culture-based study[11] (blue boxes with orange stars, **Supplementary Figure S5**). Furthermore, we found 11 other significant responses (orange boxes, **Supplementary Figure S5**) that were not detected in the isolated culture-based study[11]. including two stimulation effects, i.e. methotrexate on *Bifidobacterium longum*, and azathioprine on *Parabacteroides distasonis*.

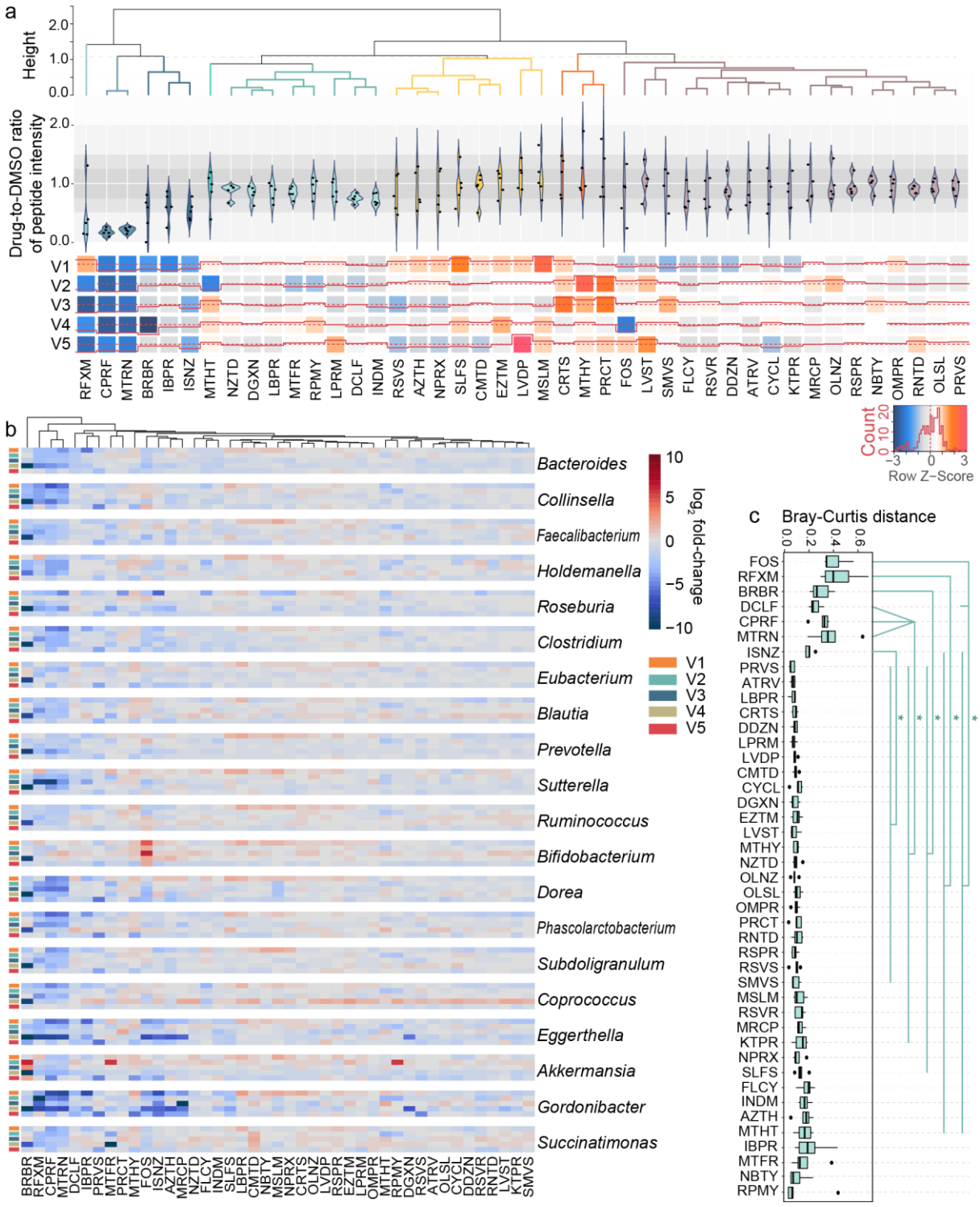

Figure 2. Response of microbiome abundance and composition to compounds. (**a**) Biomass responses of individuals' microbiomes to compounds relative to DMSO control. Ratio of peptide intensity between compound and DMSO control samples was calculated for each individual

microbiome (for full compound names, see abbreviation list in **Supplementary Table S1**). (**b**) Log_2 fold-change of genus-level biomass in response to each drug compared with the DMSO control. Top 20 most abundant genera are shown. Different color blocks in the first column indicate different individuals' microbiomes. (**c**) Bray-Curtis distance of genus-level composition between drug-treated microbiomes and the corresponding DMSO control samples. Statistical significance was calculated by pairwise Wilcoxon test (FDR-adjusted $p < 0.05$). Box spans interquartile range (25th to 75th percentile) and line within box denotes median.

Detection of three main classes of compounds

To gain a better understanding of the global effects of xenobiotics on the gut microbiome, we applied an unsupervised non-linear dimensionality reduction (NLDR) algorithm, t-distributed stochastic neighbour embedding[32], to visualize the metaproteomic data. This NLDR method converts distances between data in the original space to probabilities before visualizing on a 2-dimentional graph. NLDR analysis revealed that the 43 compounds formed three distinct classes based on their impacts on the gut microbiome functions (**Figure 3**). These 3 classes differ in the level of changes in the metaproteome. Class I compounds led to a global alteration of the metaproteome, with apparent compound-specific pattern. Class I compounds included the anti-diabetes medications berberine and metformin, the NSAID diclofenac, the prebiotic FOS, and the antibiotics ciprofloxacin, isoniazid and metronidazole. Class II compounds led to a moderate alteration of the metaproteome; these compounds included NSAIDs, histamine-2 blockers, aminosalicylates, antirheumatics and statins. Meanwhile, class III compounds had an overall weak impact on the metaproteome; these compounds included all of our tested antioxidants, antipsychotics and steroids.

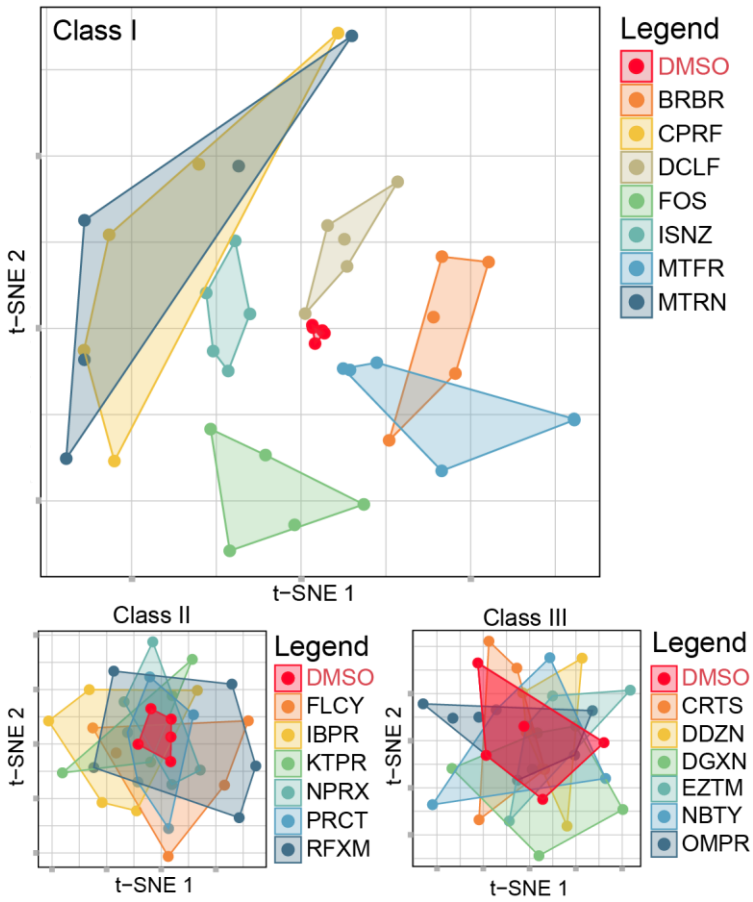

Suggested classes of compound impacts

I	II	III
BRBR	AZTH	ATRV
CPRF	CMTD	CRTS
DCLF	FLCY	CYCL
FOS	IBPR	DDZN
ISNZ	INDM	DGXN
MTFR	KTPR	EZTM
MTRN	LBPR	LPRM
	LVDP	MRCP
	LVST	MTHY
	MSLM	NBTY
	MTHT	OLNZ
	NPRX	OLSL
	NZTD	OMPR
	PRCT	RSPR
	PRVS	RSVR
	RFXM	SMVS
	RNTD	
	RPMY	
	RSVS	
	SLFS	

Figure 3. Unsupervised dimensionality reduction analysis suggesting three different classes of compound effects (for full compound names, see abbreviation list in **Supplementary Table S1**).

Gut microbiome functions are mainly altered by class I compounds

The Bray-Curtis distance of protein group profiles showed that most of the Class I compounds significantly altered the microbiome functions (**Figure 4a**). These functional alterations likely stemmed from changes in taxonomic composition as revealed by the genus-level Bray-Curtis distance analysis (**Figure 2c)**. We next examined the drug impacts on the abundance of functional categories according to clusters of orthologous groups (COG) of proteins. Class III compounds had no significant effect while classes I and II compounds significantly affected COG abundances (one-sided Wilcoxon rank sum test, FDR-adjusted $p < 0.05$; **Supplementary Figure S6**). We identified 535 COGs significantly decreased by at least one drug treatment; 15 of these COGs

were decreased by ≥ 10 compounds (**Supplementary Figure S6**). Diclofenac and FOS were the only two compounds that significantly increased COGs (55 and 81 COGs, respectively). COG categories found to be significantly enriched were responsive to 13 of the drugs tested (**Figure 4b**). Notably, 7 of the 13 drugs were class I compounds. In addition, the non-antibiotic NSAID diclofenac increased the abundance of the COG categories G (carbohydrate transport and metabolism), F (nucleotide transport and metabolism), E (amino acid transport and metabolism), and O (posttranslational modification, protein turnover, chaperones) (**Figure 4b**). Next, we mapped the significantly increased proteins from these COG categories against the string database (**Supplementary Figure S7**). Interestingly, one of the proteins that were highly connected in the string network, COG0176 – transaldolase (1.76 ± 0.21 fold-change), is involved in the biosynthesis of ansamycins, bacterial secondary metabolites that have antibiotic activities[33]. This could be part of the mechanism causing the decline in total biomass (**Figure 2a**) and shift in microbiome composition in the presence of diclofenac (**Figure 2c**).

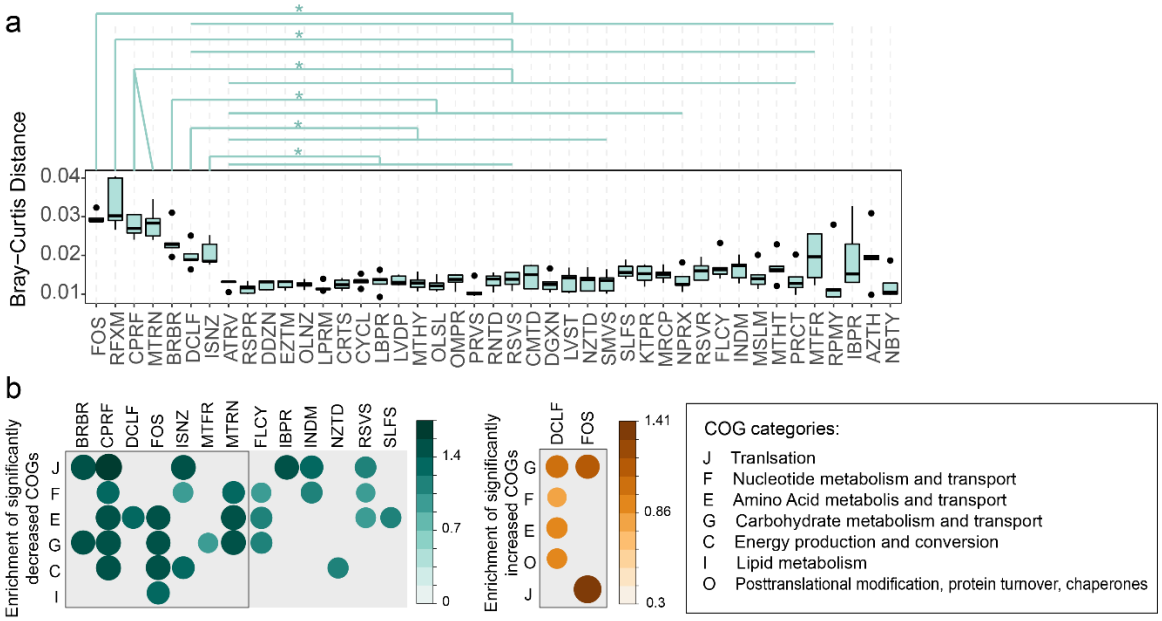

Figure 4. Effect of compounds on metaproteomic profiles of the microbiome. (**a**) Bray-Curtis distance of protein groups between drug-treated microbiomes and the corresponding DMSO control samples. Statistical significance was calculated by pairwise Wilcoxon test (FDR-adjusted $p < 0.05$). (**b**) Enrichment analysis of all significantly different COGs in the POC dataset. Significantly altered COGs with a *p*-value cutoff of 0.05 are shown.

We next analyzed the protein group intensities by partial least square discriminant analysis (PLS-DA) to determine whether metaproteomic profiles could be used to discriminate between the DMSO-control and each of the drug-treated microbiomes. PLS-DA interpretation identified drug-specific metaproteomic patterns associated with berberine, FOS, metronidazole, isoniazid, ciprofloxacin, diclofenac and rifaximin treatments (**Supplementary Figure S8**). Six of those belong to our previously identified group of class I compounds. We next performed a taxonomic analysis of the functional responses to diclofenac, FOS, ciprofloxacin, and berberine, which represent four different types of compounds (NSAID, oligosaccharide, antibiotics, anti-diabetes). Protein groups with VIP scores >1 (thereafter defined as differential proteins) were extracted from each model, and were annotated with their taxonomic and COG information. The taxonomic distributions of the differential proteins varied among drugs (**Figure 5a)**. Moreover, mapping of the differential proteins to phyla-specific pathways revealed phyla-specific responses, as shown for berberine in **Supplementary Figure S9.** In agreement with **Figure 5a,** a higher proportion of down-regulated than up-regulated pathways were identified in Firmicutes and Actinobacteria, while the opposite pattern was observed in Bacteroidetes, Proteobacteria and Verrucomicrobia. In some cases, the phylum-specific responses included up-regulation and down-regulation of different proteins within the same pathway (black lines, **Supplementary Figure S9**). For example, we observed this pattern in fatty acid, carbohydrate, and nucleotide metabolism pathways in Firmicutes.

Genus-level analysis revealed genus-specific responses to berberine (**Figure 5b**). In most genera, the genus-specific responses correlated with the overall abundance of the corresponding genus (**Figure 5b**, right panel). Nevertheless, some genera showed functional shifts in response to berberine without changes in overall abundance. For example, *Bifidobacteria*, *Roseburia*, *Eubacterium*, *Clostridium*, *Ruminococcus*, *Blautia*, and *Subdoligranulum* exhibited down-regulation of proteins in various COG categories but no changes in biomass were observed.

To assess the effects of FOS and ciprofloxacin at the enzymatic pathway level, we annotated the protein groups to KEGG enzymes. **Figure 5c** shows that FOS increased enzymes responsible for fructan and sucrose uptake, as well as enzymes for conversion of D-fructose into D-fructose-1-phosphate, D-mannose-6-phosephate and β-D-fructose-6-phosphate. FOS also affected enzymes involved in the interconversion between glutamine, glutamate and GABA (molecules involved in

gut-brain communication). In addition, enzymes involved in sulphide accumulation were affected, including decrease of dissimilatory sulfite reductase (EC 1.8.99.5) and increase of cysteine synthase (EC 2.5.1.47).

Ciprofloxacin significantly altered the levels of enzymes involved in glycolysis/glycogenesis and pentose phosphate pathways **(Figure 5c)**. The majority of enzymes involved in glycolysis were significantly increased by ciprofloxacin. Ciprofloxacin down-regulated enzymes (ECs 1.1.1.49/1.1.1.363, 3.1.1.31, 1.1.1.44/1.1.1.343) involved in synthesis of ribulose-5-phosphate, which can be isomerized to ribose 5-phosphate for nucleotide biosynthesis[34]. Moreover, the levels of antioxidant enzymes superoxide dismutase (SOD) and catalase (CAT) were increased, suggesting that ciprofloxacin induces oxidative stress in gut bacteria.

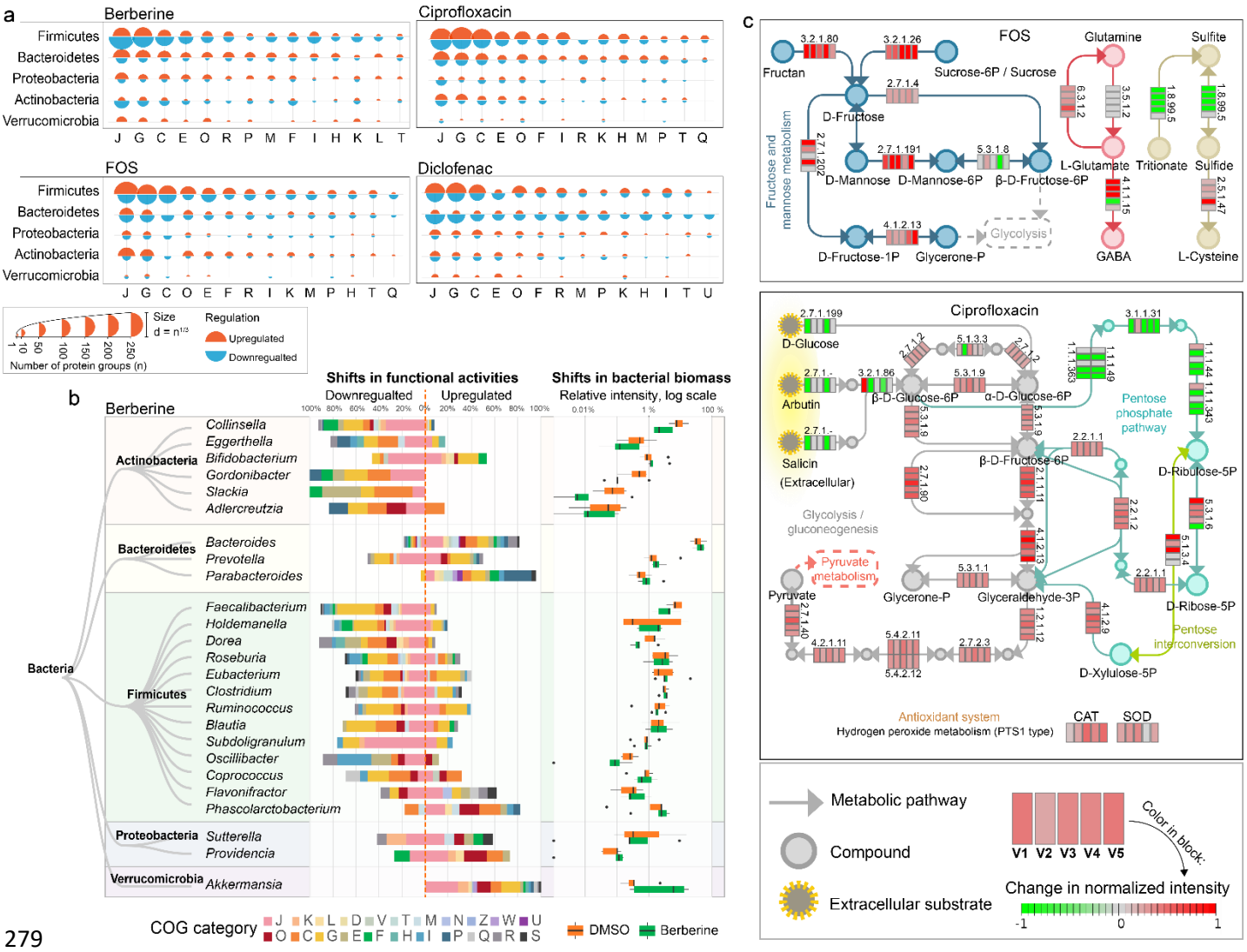

Figure 5. Global functional effects of berberine, ciprofloxacin, FOS and diclofenac (**a**) Taxon-function distribution of protein groups responding to berberine, FOS, ciprofloxacin and diclofenac. Responding protein groups were selected by partial least squares discriminant analysis (PLS-DA) based on ComBat-corrected data. The semicircle diameter represents the number of PLS-DA VIP>1 protein groups corresponding to each phyla-COG category pair. (**b**) Genus-level shifts in functional activities in response to berberine and the alterations in biomass of the corresponding genera. Functional shifts (differential protein groups) were identified by PLS-DA. For each genus, the percentages of the total numbers of up- and down-regulated protein groups corresponding to each COG category are shown. Shifts in bacterial biomass in the five microbiomes are shown in box plots with the boxes spanning interquartile range (25th to 75th percentile), and the vertical lines denoting the median for each genus. (**c**) Effect of FOS treatment on

enzymes involved in fructose and mannose metabolism, GABA production and sulfide metabolism pathways, and effect of ciprofloxacin treatment on enzymes involved in the glycolysis/gluconeogenesis and pentose phosphate pathway. The five blocks of each enzyme represent the five individual microbiomes. Colors in the blocks represent differences between normalized KEGG enzyme intensities with drug treatment versus DMSO (log_2-transformation of the original intensity followed by a quotient normalization (x/mean)).

Gut microbiome functions altered by class II compounds

Class II compounds, in contrast to class I compounds, did not cause a global shift in the microbiomes (**Figure 6a**). Indeed, we show that if analyzed on an individual sample basis (e.g. comparing cultured replicates of a single microbiome), significant individualized functional effects can be revealed (**Figure 6b and c**), suggesting high sensitivity of the RapidAIM assay in its application to personalized drug screenings. For example, we identified 303 significantly altered protein groups in cultured replicates of a single indomethacin-treated microbiome (V1). Taxon-function coupled enrichment analysis showed that down-regulated functions were highly enriched in the genus *Bacteroides*, while up-regulated functions were mostly enriched in the order Enterobacterales (**Figure 6d and e**). Increased functions of Enterobacteriales included COG0459 Chaperonin GroEL (HSP60 family) and COG0234 Co-chaperonin GroES (HSP10) (**Figure 6e**), which have been implicated in infection and diseases pathology[35].

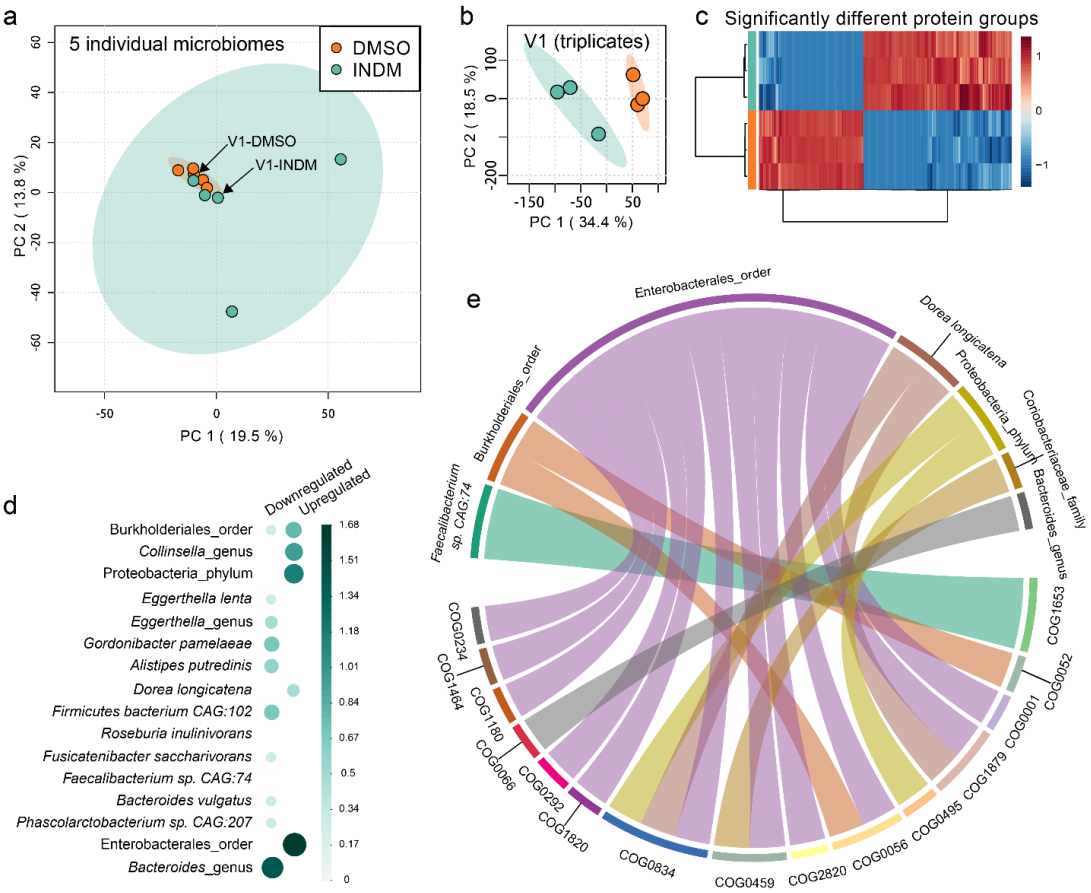

Figure 6. Individual functional responses to indomethacin. (**a**) When visualizing several individual microbiome responses with PCA (based on LFQ intensities of protein groups), inter-individual variability can be greater than drug-induced functional shifts. (**b**) PCA clearly differentiated the response of microbiome V1 treated in triplicates using RapidAIM. (**c**) 303 significant protein group responders were found by *t*-test (FDR-adjusted $p<0.05$). (**d**) Taxon enrichment analysis based on the differential protein groups, (p-adjusted=0.05). (**e**) Taxon-function coupled enrichment analysis of up-regulated protein groups.

Discussion

In the present study we developed an approach named Rapid Assay of Individual Microbiome (RapidAIM) to evaluate the effects of xenobiotics on individual microbiomes. The range of xenobiotics that reach the intestine and may interact with the gut microbiome is massive and expanding. These xenobiotics include antibiotics and other pharmaceuticals, phytochemicals,

polysaccharides, food additives and many other compounds. With the exception of antibiotics, we remain surprisingly ignorant on the extent to which these compounds affect the functions of the gut microbiome. This deficiency stems largely from the difficulty in culturing a representative gut microbial community in vitro using traditional techniques and from the lack of a rapid assay to monitor alterations in microbial functions. Here we describe a new culture technique which enables the exploration of drug-microbiome interactions using a metaproteomic approach. We validated our workflow by testing the effects of 4 antibiotics and 39 non-antibiotic compounds on the gut microbiome composition and function.

As a first step to validate RapidAIM and our metaproteomic workflow, we assessed the effect of the 43 compounds on the total microbial abundance (total biomass) and the taxon-specific biomasses. This facilitated the estimation of overall antibiotic effects, as well as changes in the abundance of beneficial and harmful bacteria in gut microbial communities. Our results suggest that the response of a bacterial species within a microbiome community could be different from its response in isolated culture. Although some of the significant responses observed in representative gut bacteria isolates[11] were replicated in our study, we identified additional responses that were not reported in bacterial isolates[11]. For example, the biomass of the opportunistic pathogen *C. difficile* was decreased by azathioprine treatment in our study, but this effect was not shown with bacterial isolates[11]. Although some differences in bacterial responses between the two studies might be due to variation at the strain level, the discrepancies suggest that the microbial community plays an important role in the response of individual microbes. As an example, community resistance mechanisms allow members of a bacterial community to survive antibiotic exposures that would be lethal to individual isolates[12].

In addition to affecting microbiome biomass, our test compounds altered metaproteomic composition. Although additional studies are needed to test a broader range of compounds, our proof of concept study has identified three different classes of drug effects on the microbiome. Seven of our 43 compounds had strong functional effects that were globally similar across different microbiomes (class I); twenty compounds caused marked functional changes in some individual microbiomes but not in others (class II); the remaining sixteen had an overall weak impact on the microbiome (class III). As expected, antibiotics in class I and class II significantly altered the microbiome. The large number of non-antibiotic drugs that were assigned to classes I

and II suggests that many drugs may cause off-target effects by altering gut microbiome composition and function. Many commonly prescribed drugs, including anti-diabetic drugs, NSAIDs, statins, histamine-2 blockers, and aminosalicylate, showed strong impacts on the *ex vivo* microbiome. It has been proposed that these compounds can induce gut microbiome changes by altering host factors such as the enterohepatic recirculation of bile acids, small intestine function, and expression of inflammatory markers[3]. Our findings show that a notable number of drugs could also directly affect the gut microbiome in the absence of a host mechanism.

We showed that the RapidAIM assay yielded insights into functional responses at multiple taxonomic levels. Using PLS-DA, we found that berberine, FOS, metronidazole, isoniazid, ciprofloxacin, diclofenac, and rifaximin all consistently shifted the metaproteome of the gut microbiome. By annotating the altered proteins at taxonomy, function and pathway levels, we revealed the actions of the different drugs on the microbiome. For example, FOS treatment elevated enzymes involved in fructan and sucrose uptake, as well as enzymes involved in the interconversion among glutamine, glutamate and GABA, which are associated with microbiome communication via the gut–brain axis[36]. In agreement, a study has shown that FOS administration increased GABA receptor genes in mice, and further exhibited both antidepressant and anxiolytic effects[37]. FOS also decreased proteins involved in sulfide generation, suggesting decreased sulfide accumulation in the microbiome. This observation is in agreement with *in vivo* studies showing that FOS treatment decreased the concentration of fecal H_2S[29,38,39]. Ciprofloxacin treatment increased enzymes SOD and CAT, which was in agreement with several reports indicating that ciprofloxacin triggers oxidative stress in several bacteria[40-42]. With berberine treatment, we showed that taxon-specific functional shifts can occur either with or without a change in the taxon's biomass. This observation highlights the strength of our workflow which enables quantitative metaproteomic profiling of the microbiome. Indeed, current classical sequencing-based approaches (16S rDNA or metagenomics sequencing), which generate relative abundances, would not detect these types of changes.

An impressive range of pharmaceuticals reaches the intestine and interacts with the gut microbiome. To date, the field of drug-microbiome interactions largely focuses on microbial drug metabolism, with a limited understanding of the effects of pharmaceuticals on the

composition and function of the gut microbiome. A better understanding of these interactions is essential given that the drug effects on the microbiome might have important health consequences. Here, we build a workflow named Rapid Assay of Individual Microbiome (RapidAIM) for the functional profiling of drug effects on the gut microbiome. This workflow consists of a culture-based assay coupled to metaproteomic analysis. We have shown that our workflow is robust, reproducible and quantitative. Importantly, quantitative functional profiling out-performs relative analyses (e.g. classical 16S rDNA and metagenome sequencing) which are limited in their ability to reveal direct drug effects on the microbiome. However, our workflow also exhibits certain limitations. In particular, MS analysis is a time-consuming process not well suited for high-throughput screening. To this end, a fast-pass screening process such as tandem mass tags (TMT)[43,44] could be used to multiplex multiple microbiome samples in one MS analysis. Furthermore, our workflow only measures the direct effects of compounds on the microbiome. In its current implementation, it does not take into account the host effect on the microbiome and/or the effects of drug metabolites produced by the host. Future efforts could be aimed at incorporating co-culture of host cells/tissue and gut bacteria[45,46] into a high-throughput drug screening process for achieving more comprehensive insights on host-drug-microbiome interaction. RapidAIM could also be coupled with techniques such as metagenomics or metabolomics to obtain a more comprehensive view of the microbiome interaction with various drugs.

Methods

Stool sample preparation

The Research Ethics Board protocol (# 20160585-01H) for stool sample collection was approved by the Ottawa Health Science Network Research Ethics Board at the Ottawa Hospital. Stool samples were obtained from 5 healthy volunteers (age range 27 - 36 years; 3 males and 2 females). Exclusion criteria were: IBS, IBD, or diabetes diagnosis; antibiotic use or gastroenteritis episode in the last 3 months; use of pro-/pre-biotic, laxative, or anti-diarrheal drugs in the last month; or pregnancy. All volunteers were provided with a stool collection kit, which included a 50 ml Falcon tube containing 15 ml of sterile phosphate-buffered saline (PBS)

pre-reduced with 0.1% (w/v) L-cysteine hydrochloride, a 2.5 ml sterile sampling spoon (Bel-Art, United States), plastic wrap, gloves and disposal bags. Briefly, each volunteer placed the plastic wrap over a toilet to prevent the stool from contacting water, collected ~3 g of stool with the sampling spoon, and dropped the spoon into the prepared 50 ml tube. The sample was immediately weighed by a researcher and transferred into an anaerobic workstation (5% H_2, 5% CO_2, and 90% N_2 at 37 ℃), where the tube was uncapped to remove O_2 before homogenization with a vortex mixer. Then the homogenate was filtered using sterile gauzes to remove large particles and obtain the microbiome inoculum.

Culturing of microbiomes and drug treatments

Each microbiome inoculum was immediately inoculated at a concentration of 2% (w/v) into a 96-well deep well plate containing 1 ml culture medium and a compound dissolved in 5 µl DMSO (or 5 µl DMSO as the control) in each well. We used an optimized culture medium composition that can maintain the composition and taxon-specific functional activities of individual gut microbiomes (paper under review). The culture medium was sterile and had been pre-reduced overnight in an anaerobic workstation. Concentration of each compound was determined based on the assumption that maximal oral dosage of the drug distributed in 200 g average weight of the colon contents. However, several compounds (i.e. cimetidine, ciprofloxacin, flucytosine, mesalamine, metformin, metronidazole, naproxen-sodium, paracetamol, rifaximin, sodium butyrate, and sulfalazine) exceeded solubility in the given volume of DMSO (5 µl). After confirming that these compounds still showed effect after a 10× dilution (as can be seen from hierarchical clustering in **Supplementary Figure S3**), the concentrations corresponding to the 1/10 highest oral dosages were used for these compounds. Detailed catalogue number and concentration of each compound is listed in **Supplementary Table S1**. After inoculation, the 96-well deep well plate was covered with a sterile silicone gel mat with a vent hole for each well made by a sterile syringe needle. Then, the plate was shaken at 500 rpm with a digital shaker (MS3, IKA, Germany) at 37ºC for 24 hours in the anaerobic chamber.

Metaproteomic sample processing and LC-MS/MS analysis

We used a previously reported metaproteomic sample processing workflow[18], adapted for microplates. After culturing for 24 hr, each 96-well plate was transferred out of the anaerobic station and was immediately centrifuged at 300 g for 5 min to remove debris. The supernatants

were transferred into new 96-well deep well plates for another two rounds of debris removal at 300 g. The supernatants were then transferred to a new plate and centrifuged at 2,272 g for 1 hr to pellet the microbiome. The supernatant was removed and the pelleted bacterial cells were washed three times with cold PBS in the same 96-deep well plate, pelleting the cells after each wash by a 2,272 g centrifugation for 1 hr. The 96-well plate containing harvested bacterial cells was then stored overnight at -80°C before bacterial cell lysis and protein extraction. The lysis buffer was freshly prepared, containing 8 M urea in 100 mM Tris-HCl buffer (pH = 8.0), plus Roche PhosSTOP™ and Roche cOmplete™ Mini tablets. Microbial cell pellets were then re-suspended in 150 μl lysis buffer and lysed on ice using a sonicator (Q125 Qsonica, USA) with an 8-tip-horn probe. 100% amplitude was used (i.e. 15.6 Watts per sample), and four cycles of 30 s ultrasonication and 30 s cooling down were performed. Protein concentrations of the DMSO control samples were measured in triplicate using a detergent compatible (DC) assay (Bio-Rad, USA). Then, a volume equivalent to the average volume of 50 μg of protein in the DMSO control samples was acquired from each sample and placed into a new 96-deep well plate. The samples were reduced and alkylated with 10 mM dithiothreitol (DTT) and 20 mM iodoacetamide (IAA), followed by a 10× dilution using 100 mM Tris-HCl (pH = 8.0) and tryptic digestion under 37 ℃ for 18 hr using 1 μg of trypsin per well (Worthington Biochemical Corp., Lakewood, NJ). Digested peptides were desalted using a panel of lab-made 96-channel filter tips generated by inserting 96 20 μl filter tips into a 96-well cover mat and stacking each filter tip with 5 mg of 10-μm C18 column beads. After being washed twice with 0.1% formic acid (v/v), tryptic peptides were then eluted with 80% acetonitrile (v/v)/0.1% formic acid (v/v).

After freeze-drying, each sample was re-dissolved in 100 μl 0.1% formic acid (v/v), and 2 μl of the solution (corresponding to 1 μg of proteins in the DMSO control) was loaded for LC-MS/MS analysis in a randomized order. An Agilent 1100 Capillary LC system (Agilent Technologies, San Jose, CA) and a Q Exactive mass spectrometer (ThermoFisher Scientific Inc.) were used. Peptides were separated with a tip column (75 μm inner diameter × 50 cm) packed with reverse phase beads (1.9 μm/120 Å ReproSil-Pur C18 resin, Dr. Maisch GmbH, Ammerbuch, Germany) following a 90 min gradient from 5 to 30% (v/v) acetonitrile at a 200 nL/min flow rate. 0.1% (v/v) formic acid in water was used as solvent A, and 0.1% FA in 80% acetonitrile was used as solvent B. The MS scan was performed from 300 to 1800 m/z, followed by data-dependent

MS/MS scan of the 12 most intense ions, a dynamic exclusion repeat count of two, and repeat exclusion duration of 30 s.

Assessment of the metaproteomic workflow

Microplate-based metaproteomic sample preparation:

Due to a few differences in the metaproteomic procedure compared with previously published tube-based ones[47,48], we examined the effect of protocol differences on sample quality at each step. Detailed procedures are described in **Supplementary Figure S1**.

Equal-volume strategy:

Six dilutions of a single microbiome sample were prepared in triplicate wells and an equal volume was taken from each sample for tryptic digestion and LC-MS/MS analysis. Metaproteomic sample processing and analysis followed the same procedures stated above, and total peptide intensity was calculated. A DC protein concentration assay was also performed with each sample. Linearity between total protein concentration and total peptide intensity quantified by LC-MS/MS was then compared.

Metaproteomics data analysis

Metaproteomic database search:

Protein/peptide identification and quantification, taxonomic assignment and functional annotations were done using the MetaLab software (version 1.1.0)[49]. MetaLab is a software that automates an iterative database search strategy, i.e. MetaPro-IQ[48]. The search was based on a human gut microbial gene catalog containing 9,878,647 sequences from http://meta.genomics.cn/. A spectral clustering strategy were used for database construction from all raw files, then the peptide and protein lists were generated by applying strict filtering based on a FDR of 0.01, and quantitative information of proteins were obtained with the maxLFQ algorithm on MaxQuant (version 1.5.3.30). Carbamidomethyl (C) was set as a fixed modification and oxidation (M) and N-terminal acetylation (Protein N-term) were set as variable modifications. Instrument resolution was set as “High-High”.

Microbiome biomass analyses:

Total microbiome biomass was estimated for each sample by summing peptide intensities. Taxonomic identification was achieved by assigning peptide sequences with lineage of lowest

common ancestor (LCA). The "peptide to taxonomy" database (pep2tax database) was selected for mapping identified peptides to the taxonomic lineages[49]. Bacteria, eukaryota, viruses, and archaea were included in the LCA calculation. Taxonomic biomass was quantified by summing the intensities of the peptides corresponding to each taxon. A Bray-Curtis dissimilarity-based approach[30] was applied for evaluating the variation of genus-level biomass contributions between drug-treated and DMSO control groups. Calculation of the Bray-Curtis distance was performed using the R package "vegan"[31].

Functional analysis:

The quantified protein groups were first filtered according to the criteria that the protein appears in >80% of the microbiomes with at least one drug treatment. Then LFQ protein group intensities of the filtered file was $\log_2$-transformed and normalized through quotient transformation (x/mean) using the R package clusterSim. Then, LFQ protein group intensities were processed by a ComBat process[50,51] using iMetalab.ca[52] to remove possible batch effects between individual microbiomes. Using the ComBat-corrected data, an unsupervised non-linear dimensionality reduction algorithm, t-distributed stochastic neighbor embedding (t-SNE)[32] was then applied to visualize similarities between samples using the R package Rtsne. Parameter for the function Rtsne() were, perplexity=10, max_iter = 1200 (number of iterations), other parameters were set as default. The R function geom_polygon implemented in ggplot2 was used to visualize the t-SNE results. t-SNE visualizations (using random seeds) were carried out with subgroups of 6 random compounds plus the DMSO control. Through repeatedly (≥5 repeats) running t-SNE with each subgroup, compounds with different clustering performances (compared to the DMSO cluster, **Figure 3**) were categorized into three classes. Figures were then regenerated with the three classes of compounds. For a clearer visualization, six randomly selected compounds from classes II and III were shown, respectively.

Functional annotations of protein groups, including COG and KEGG information, were obtained in the MetaLab software. In addition, KEGG ortholog (KO) annotation of protein FASTA sequences was conducted using GhostKOALA (https://www.kegg.jp/ghostkoala/)[53]. Log_2 fold-change of each drug-treated sample relative to the corresponding DMSO control was calculated using the abundances of proteins annotated to COG categories and COGs. Functional enrichment

analysis was performed using the enrichment module on iMetalab.ca[52] through inputting the list of COG functional proteins. Adjusted *p*-value cutoff was set at 0.05 for the enrichment analysis.

Statistical analysis:

We examined data distribution on all levels of data, and results indicated non-normal distributions of the dataset (examples shown in **Supplementary Figures S10 and 11**). Hence, a non-parametric statistical hypothesis test, the Wilcoxon rank sum test, was applied in statistical analyses. For multiple comparisons, *p*-values were adjusted using the Benjamini-Hochberg false discovery rate (FDR) procedure[54]. For multivariate analysis, partial least-squares discriminant analyses (PLS-DA) based on ComBat-corrected protein group intensities were performed using MetaboAnalyst (http://www.metaboanalyst.ca/)[55]. PLS-DA model were evaluated by cross-validation of R^2 and Q^2.

Data visualizations:

Box plots, violin plots, hierarchical clusterings, 3D scatter plots, heatmaps, PCA, and t-SNE were visualized using R packages ggplot2, gridExtra, scatterplot3d, and pheatmap. Pathway maps were visualized using iPATH 3 (https://pathways.embl.de/)[56], Pathview Web (https://pathview.uncc.edu/)[57] and Adobe Illustrator. PLS-DA score plots were visualized on MetaboAnalyst 4.0 (http://www.metaboanalyst.ca/)[55]. Stacked column bars, ComBat results, and functional enrichments were visualized on iMetaLab.ca[52].

Supplementary information

Supplementary tables S1-S2.

Supplementary figures S1-S11.

Acknowledgments

This work was supported by the Government of Canada through Genome Canada and the Ontario Genomics Institute (OGI-114 and OGI-149), CIHR grant (ECD-144627), the Natural Sciences and Engineering Research Council of Canada (NSERC, grant no. 210034), and the Ontario Ministry of Economic Development and Innovation (REG1-4450). The authors wish to thank Dr. Kendra Hodgkinson for editing the manuscript.

Author contributions

D.F., A.S. and L.L. designed the study. J.M. coordinated the volunteers and collected the samples. L.L., X.Z. and Z.N. developed the workflow and performed the experiments. L.L., Z.N., X.Z. and K.C. analyzed and visualized the data. L.L, D.F. and A.S. wrote the manuscript. All authors read and approved the final manuscript.

Competing interests

D.F. and A.S. have co-founded Biotagenics and MedBiome, clinical microbiomics companies. All other authors declare no competing interests.

Reference

1. Lynch, S.V. & Pedersen, O. The Human Intestinal Microbiome in Health and Disease. *New England Journal of Medicine* **375**, 2369-2379 (2016).
2. Jia, W., Li, H., Zhao, L. & Nicholson, J.K. Gut microbiota: a potential new territory for drug targeting. *Nature Reviews Drug Discovery* **7**, 123 (2008).
3. Le Bastard, Q., *et al.* Systematic review: human gut dysbiosis induced by non-antibiotic prescription medications. *Alimentary Pharmacology & Therapeutics* **47**, 332-345 (2017).
4. Urquhart, L. FDA new drug approvals in Q2 2018. *Nature Reviews Drug Discovery* **17**, 536 (2018).
5. Harvey, A.L., Edrada-Ebel, R. & Quinn, R.J. The re-emergence of natural products for drug discovery in the genomics era. *Nature Reviews Drug Discovery* **14**, 111 (2015).
6. McDonald, J.A.K., *et al.* Evaluation of microbial community reproducibility, stability and composition in a human distal gut chemostat model. *Journal of Microbiological Methods* **95**, 167-174 (2013).
7. Van den Abbeele, P., *et al.* Butyrate-producing Clostridium cluster XIVa species specifically colonize mucins in an in vitro gut model. *The Isme Journal* **7**, 949 (2012).
8. Van de Wiele, T., Van den Abbeele, P., Ossieur, W., Possemiers, S. & Marzorati, M. The Simulator of the Human Intestinal Microbial Ecosystem (SHIME®). in *The Impact of Food Bioactives on Health: in vitro and ex vivo models* (eds. Verhoeckx, K., *et al.*) 305-317 (Springer International Publishing, Cham, 2015).
9. McDonald, J.A.K., *et al.* Evaluation of microbial community reproducibility, stability and composition in a human distal gut chemostat model. *J Microbiol Methods* **95**, 167 (2013).
10. Kim, B.-S., Kim, J.N. & Cerniglia, C.E. *In vitro* culture conditions for maintaining a complex population of human gastrointestinal tract microbiota. *Journal of Biomedicine and Biotechnology* **2011**, 10 (2011).
11. Maier, L., *et al.* Extensive impact of non-antibiotic drugs on human gut bacteria. *Nature* **555**, 623 (2018).
12. Vega, N.M. & Gore, J. Collective antibiotic resistance: mechanisms and implications. *Current Opinion in Microbiology* **21**, 28-34 (2014).
13. Ranjan, R., Rani, A., Metwally, A., McGee, H.S. & Perkins, D.L. Analysis of the microbiome: Advantages of whole genome shotgun versus 16S amplicon sequencing. *Biochemical and biophysical research communications* **469**, 967-977 (2016).

14. Bashiardes, S., Zilberman-Schapira, G. & Elinav, E. Use of Metatranscriptomics in Microbiome Research. *Bioinformatics and biology insights* **10**, 19-25 (2016).
15. Zhang, X., *et al.* Deep metaproteomics approach for the study of human microbiomes. *Anal Chem* **89**, 9407-9415 (2017).
16. Zhang, X., *et al.* Metaproteomics reveals associations between microbiome and intestinal extracellular vesicle proteins in pediatric inflammatory bowel disease. *Nature Communications* **9**, 2873 (2018).
17. Kleiner, M., *et al.* Assessing species biomass contributions in microbial communities via metaproteomics. *Nature Communications* **8**, 1558 (2017).
18. Zhang, X., *et al.* Assessing the impact of protein extraction methods for human gut metaproteomics. *Journal of Proteomics* **180**, 120-127 (2018).
19. Zhang, X., *et al.* MetaPro-IQ: a universal metaproteomic approach to studying human and mouse gut microbiota. *Microbiome* **4**, 31 (2016).
20. Cheng, K., *et al.* MetaLab: an automated pipeline for metaproteomic data analysis. *Microbiome* **5**, 157 (2017).
21. Zhang, X., *et al.* Deep Metaproteomics Approach for the Study of Human Microbiomes. *Analytical Chemistry* **89**, 9407-9415 (2017).
22. Namasivayam, S., *et al.* Longitudinal profiling reveals a persistent intestinal dysbiosis triggered by conventional anti-tuberculosis therapy. *Microbiome* **5**, 71 (2017).
23. Liang, X., *et al.* Bidirectional interactions between indomethacin and the murine intestinal microbiota. *eLife* **4**, e08973 (2015).
24. Hustoft, T.N., *et al.* Effects of varying dietary content of fermentable short-chain carbohydrates on symptoms, fecal microenvironment, and cytokine profiles in patients with irritable bowel syndrome. *Neurogastroenterology & Motility* **29**, e12969 (2016).
25. Lee, H., *et al.* Modulation of the gut microbiota by metformin improves metabolic profiles in aged obese mice. *Gut Microbes* **9**, 155-165 (2018).
26. Zhu, L., *et al.* Berberine treatment increases Akkermansia in the gut and improves high-fat diet-induced atherosclerosis in Apoe−/− mice. *Atherosclerosis* **268**, 117-126 (2018).
27. Zhang, X., *et al.* Structural Changes of Gut Microbiota during Berberine-Mediated Prevention of Obesity and Insulin Resistance in High-Fat Diet-Fed Rats. *PLOS ONE* **7**, e42529 (2012).
28. Shin, N.-R., *et al.* An increase in the Akkermansia spp. population induced by metformin treatment improves glucose homeostasis in diet-induced obese mice. *Gut* (2013).
29. Kawaguchi, M., Tashiro, Y., Adachi, T. & Tamura, Z. Changes in Intestinal Condition, Fecal Microflora and Composition of Rectal Gas after Administration of Fructooligosaccharide and Lactulose at Different Doses. *Bifidobacteria and Microflora* **12**, 57-67 (1993).
30. The Human Microbiome Project, C. Structure, function and diversity of the healthy human microbiome. *Nature* **486**, 207 (2012).
31. Oksanen, J., *et al.* vegan: Community Ecology Package. R package version 2.5-1. https://CRAN.R-project.org/package=vegan. (2018).
32. Maaten, L.J.P.v.d. & Hinton, G.E. Visualizing high-dimensional data using t-SNE. *Journal of Machine Learning Research* **9**, 2579-2605 (2008).
33. Rinehart, K.L. & Shield, L.S. Chemistry of the Ansamycin Antibiotics. in *Fortschritte der Chemie Organischer Naturstoffe / Progress in the Chemistry of Organic Natural Products* (eds. Cimino, G., *et al.*) 231-307 (Springer Vienna, Vienna, 1976).
34. Mayes, P.A. & Bender, D.A. The pentose phosphate pathway & other pathways of hexose metabolism. in *Harper's illustrated biochemistry* (eds. Murray, R.K., Granner, D.K., Mayes, P.A. & Rodwell, V.W.) 163-172 (Lange Medical Books/McGraw-Hill, New York, 2003).
35. Ranford, J.C. & Henderson, B. Chaperonins in disease: mechanisms, models, and treatments. *Molecular Pathology* **55**, 209-213 (2002).

36. Cryan, J.F. & Dinan, T.G. Mind-altering microorganisms: the impact of the gut microbiota on brain and behaviour. *Nature Reviews Neuroscience* **13**, 701 (2012).
37. Burokas, A., *et al.* Targeting the Microbiota-Gut-Brain Axis: Prebiotics Have Anxiolytic and Antidepressant-like Effects and Reverse the Impact of Chronic Stress in Mice. *Biological Psychiatry* **82**, 472-487 (2017).
38. Swanson, K.S., *et al.* Fructooligosaccharides and Lactobacillus acidophilus Modify Gut Microbial Populations, Total Tract Nutrient Digestibilities and Fecal Protein Catabolite Concentrations in Healthy Adult Dogs. *The Journal of Nutrition* **132**, 3721-3731 (2002).
39. Lei, X.J., Cheong, J.Y., Park, J.H. & Kim, I.H. Supplementation of protease, alone and in combination with fructooligosaccharide to low protein diet for finishing pigs. *Animal Science Journal* **88**, 1987-1993 (2017).
40. Albesa, I., Becerra, M.C., Battán, P.C. & Páez, P.L. Oxidative stress involved in the antibacterial action of different antibiotics. *Biochemical and Biophysical Research Communications* **317**, 605-609 (2004).
41. Becerra, M.C. & Albesa, I. Oxidative stress induced by ciprofloxacin in Staphylococcus aureus. *Biochemical and Biophysical Research Communications* **297**, 1003-1007 (2002).
42. Becerra, M.C., Páez, P.L., Laróvere, L.E. & Albesa, I. Lipids and DNA oxidation in Staphylococcus aureus as a consequence of oxidative stress generated by ciprofloxacin. *Molecular and Cellular Biochemistry* **285**, 29-34 (2006).
43. Guirro, M., *et al.* Multi-omics approach to elucidate the gut microbiota activity: Metaproteomics and metagenomics connection. *ELECTROPHORESIS* **39**, 1692-1701 (2018).
44. Thompson, A., *et al.* Tandem Mass Tags: A Novel Quantification Strategy for Comparative Analysis of Complex Protein Mixtures by MS/MS. *Analytical Chemistry* **75**, 1895-1904 (2003).
45. Shah, P., *et al.* A microfluidics-based in vitro model of the gastrointestinal human–microbe interface. *Nature Communications* **7**, 11535 (2016).
46. Kim, H.J., Lee, J., Choi, J.-H., Bahinski, A. & Ingber, D.E. Co-culture of Living Microbiome with Microengineered Human Intestinal Villi in a Gut-on-a-Chip Microfluidic Device. *Journal of visualized experiments : JoVE*, 54344 (2016).
47. Li, L., *et al.* Evaluating in Vitro Culture Medium of Gut Microbiome with Orthogonal Experimental Design and a Metaproteomics Approach. *Journal of Proteome Research* **17**, 154-163 (2018).
48. Zhang, X., *et al.* In Vitro Metabolic Labeling of Intestinal Microbiota for Quantitative Metaproteomics. *Analytical Chemistry* **88**, 6120-6125 (2016).
49. Cheng, K., *et al.* MetaLab: an automated pipeline for metaproteomic data analysis. *Microbiome* **5**, 157 (2017).
50. Nyamundanda, G., Poudel, P., Patil, Y. & Sadanandam, A. A Novel Statistical Method to Diagnose, Quantify and Correct Batch Effects in Genomic Studies. *Scientific Reports* **7**, 10849 (2017).
51. Chen, C., *et al.* Removing Batch Effects in Analysis of Expression Microarray Data: An Evaluation of Six Batch Adjustment Methods. *PLOS ONE* **6**, e17238 (2011).
52. Liao, B., *et al.* iMetaLab 1.0: a web platform for metaproteomics data analysis. *Bioinformatics*, bty466-bty466 (2018).
53. Kanehisa, M., Sato, Y. & Morishima, K. BlastKOALA and GhostKOALA: KEGG Tools for Functional Characterization of Genome and Metagenome Sequences. *Journal of Molecular Biology* **428**, 726-731 (2016).
54. Benjamini, Y. & Hochberg, Y. Controlling the False Discovery Rate: A Practical and Powerful Approach to Multiple Testing. *Journal of the Royal Statistical Society. Series B (Methodological)* **57**, 289-300 (1995).
55. Chong, J., *et al.* MetaboAnalyst 4.0: towards more transparent and integrative metabolomics analysis. *Nucleic Acids Research* **46**, W486-W494 (2018).

56. Yamada, T., Letunic, I., Okuda, S., Kanehisa, M. & Bork, P. iPath2.0: interactive pathway explorer. *Nucleic Acids Research* **39**, W412-W415 (2011).
57. Luo, W., Pant, G., Bhavnasi, Y.K., Blanchard, J.S.G. & Brouwer, C. Pathview Web: user friendly pathway visualization and data integration. *Nucleic Acids Research* **45**, W501-W508 (2017).

RapidAIM: An in-depth assay for comprehensive analysis of individual microbiome responses to drugs

Leyuan Li[1], Zhibin Ning[1], Xu Zhang[1], Janice Mayne[1], Kai Cheng[1], Alain Stintzi*[1], Daniel Figeys[*1,2,3]

[1] Department of Biochemistry, Microbiology and Immunology, Ottawa Institute of Systems Biology, Faculty of Medicine, University of Ottawa, Ottawa, Canada

[2] Department of Chemistry and Biomolecular Sciences, University of Ottawa, Ottawa, Canada

[3] Canadian Institute for Advanced Research, Toronto, Canada

* Corresponding Authors, Email: dfigeys@uottawa.ca (DF), and astintzi@uottawa.ca (AS)

Supplementary figures

Figure S1. Establishment and step-by-step validation of the microplate-based metaproteomic sample preparation workflow of the RapidAIM assay

Figure S2. Assessment of the equal-volume digestion and LC-MS/MS analysis strategy

Figure S3. Reproducibility of RapidAIM assay on different levels

Figure S4. *In vitro* taxonomic responses to drugs reported in *in vivo* studies

Figure S5. Comparison of species responses between RapidAIM POC and a pure culture-based study

Figure S6. Log_2 fold-change of functions at the COG protein level

Figure S7. String interaction of COG functional proteins significantly stimulated by diclofenac

Figure S8. Score plots and cross-validations of seven PLS-DA models

Figure S9. Phylum-specific functional responses to Berberine

Figure S10. Randomly selected LFQ intensities of protein groups showing heavy tailed distribution on the Q-Q plots

Figure S11. Randomly selected log2-fold changes of COGs showing heavy tailed distribution on the Q-Q plots

Supplementary Figure S1

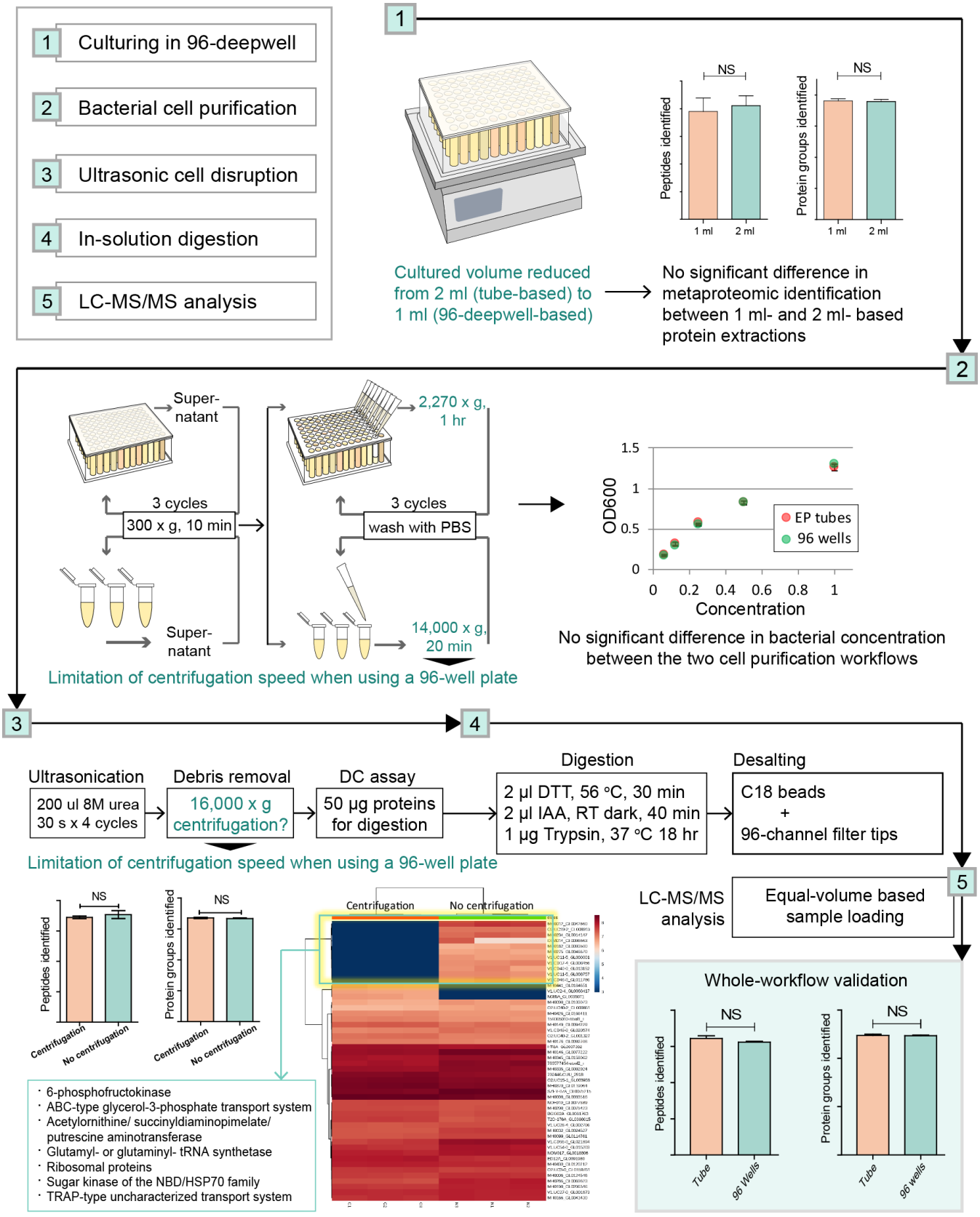

Figure S1. Establishment and step-by-step validation of the microplate-based metaproteomic sample preparation workflow of the RapidAIM assay.

After culturing in a 96-well deepwell plate **[1]**, the bacterial cells were washed with PBS **[2]**, then disrupted with four cycles of 30 s ultrasonication **[3]**. Protein concentration was measured in the DMSO control sample using a DC protein assay. This concentration was used to calculate a volume equivalent to 50 μg proteins in the control sample. This volume was taken from every sample and digested with trypsin **[4]**, then desalted with a panel of 96 filter tips packed with C18 beads and equal volumes of each sample were analyzed by LC-MS/MS **[5]**.

Due to a few differences in the metaproteomic procedure compared with tube-based protocols, we examined the effect of protocol differences on sample quality step-by-step. In previously published protocols, samples were cultured in 2 ml culture tubes [1,2]. In step **[1]**, culturing samples in a 96-well plate reduced the sample size to 1 ml. No significant difference was shown by *t*-test in peptide and protein group identification numbers between protein extractions from 1 ml and 2 ml samples. For step **[2]**, the 96-deepwell plates limited centrifugation speed to 2,270 g (versus 14,000 g in the original protocol), so we extended the centrifugation time from 20 min to 1 hour and tested whether bacterial concentration was affected by the altered centrifugation process[1,3]. Concentration of purified bacterial cells were compared by OD_{600} after being re-suspended in 1 ml, 2 ml, 4 ml, 8 ml, and 16 ml PBS. No significant difference in OD_{600} reads was observed between the two cell purification protocols. In step **[3]**, the original protocol used a high-speed centrifugation (16,000 g) to remove cell debris after the ultrasonication. Due to the limitation of centrifugation speed when using a microplate, we compared metaproteomic profiles of the sample when digested with or without cell debris removal. No significant differences were found in the number of protein identifications. In terms of differentially identified proteins, we found that the samples without cell debris removal resulted in more identifications of cell-membrane proteins such as the ABC-type transport systems, as well as cytoskeleton-related proteins, such as the translation elongation factor EF-Tu [4,5], 6-phosphofructokinase [6], and ribosomes [7]. Therefore, we infer that eliminating the centrifugation process could reduce the removal of cytoskeleton and cell membrane proteins. For step **[4]**, no validation was necessary as the same type of filter tips were used in both protocols. Finally, we performed a whole-workflow comparison of the metaproteomic outcomes between traditional tube-based and 96-well-based processes. The microplate-based metaproteomic workflow showed no statistically significant difference in peptide and protein identification compared with the tube-based workflow.

Supplementary Figure S2

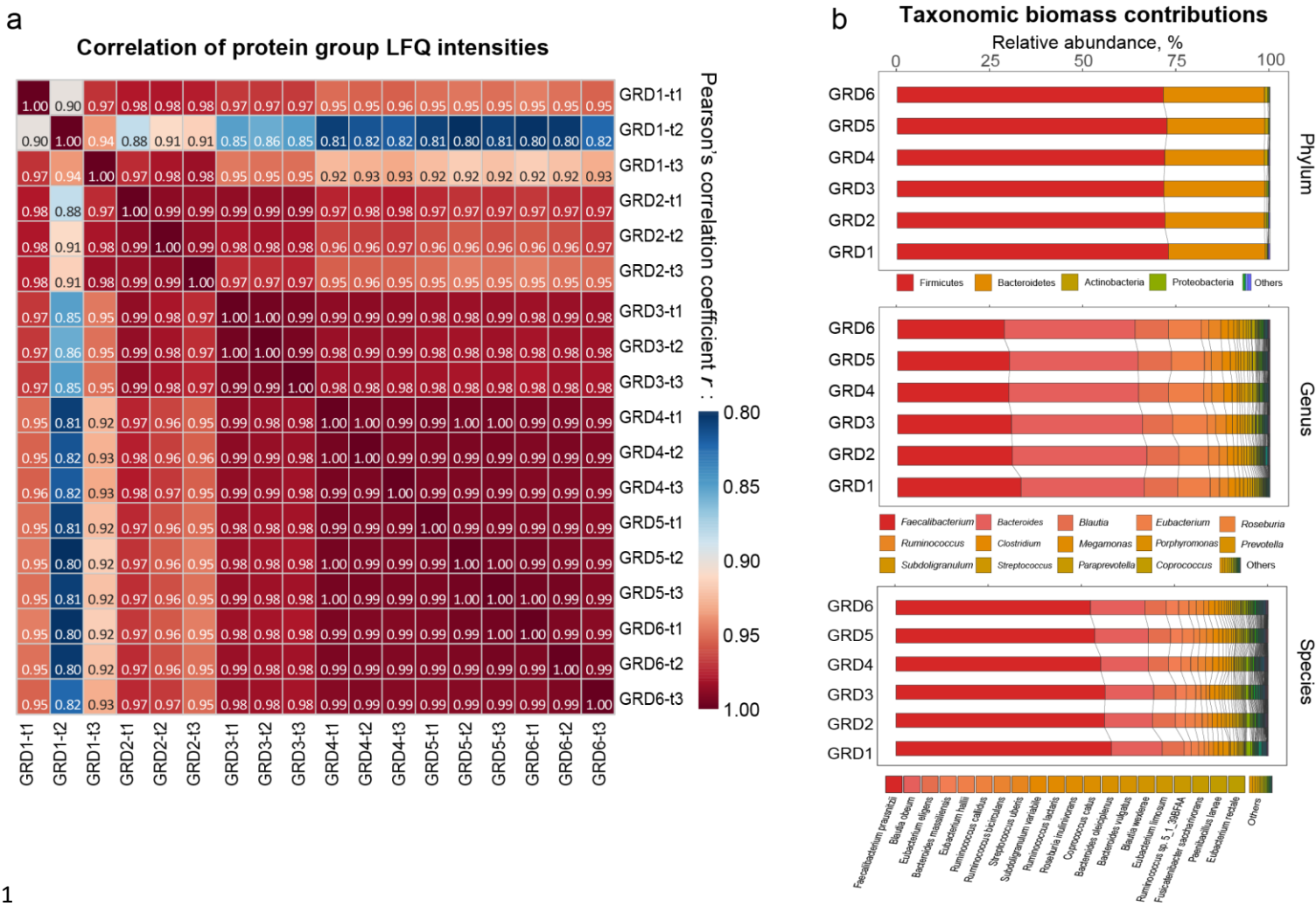

Figure S2. Assessment of the equal-volume digestion and LC-MS/MS analysis strategy.
(**a**) In triplicates, six dilutions of a single microbiome sample were subjected to this equal-volume based analysis.
The LFQ intensities of protein groups showed Pearson's correlation coefficient $r > 0.95$ between most dilutions, but a lower r was seen in the samples with the lowest concentration. (**b**) Comparison of taxonomic biomass contributions on different levels (summed peptide intensity assigned to different taxa) among diluted groups suggested very low level of bias. GRD1-6 are six different dilution gradients (protein concentration shown in Figure 1b), and t1-t3 are technical replicates of the same conditions.

Supplementary Figure S3

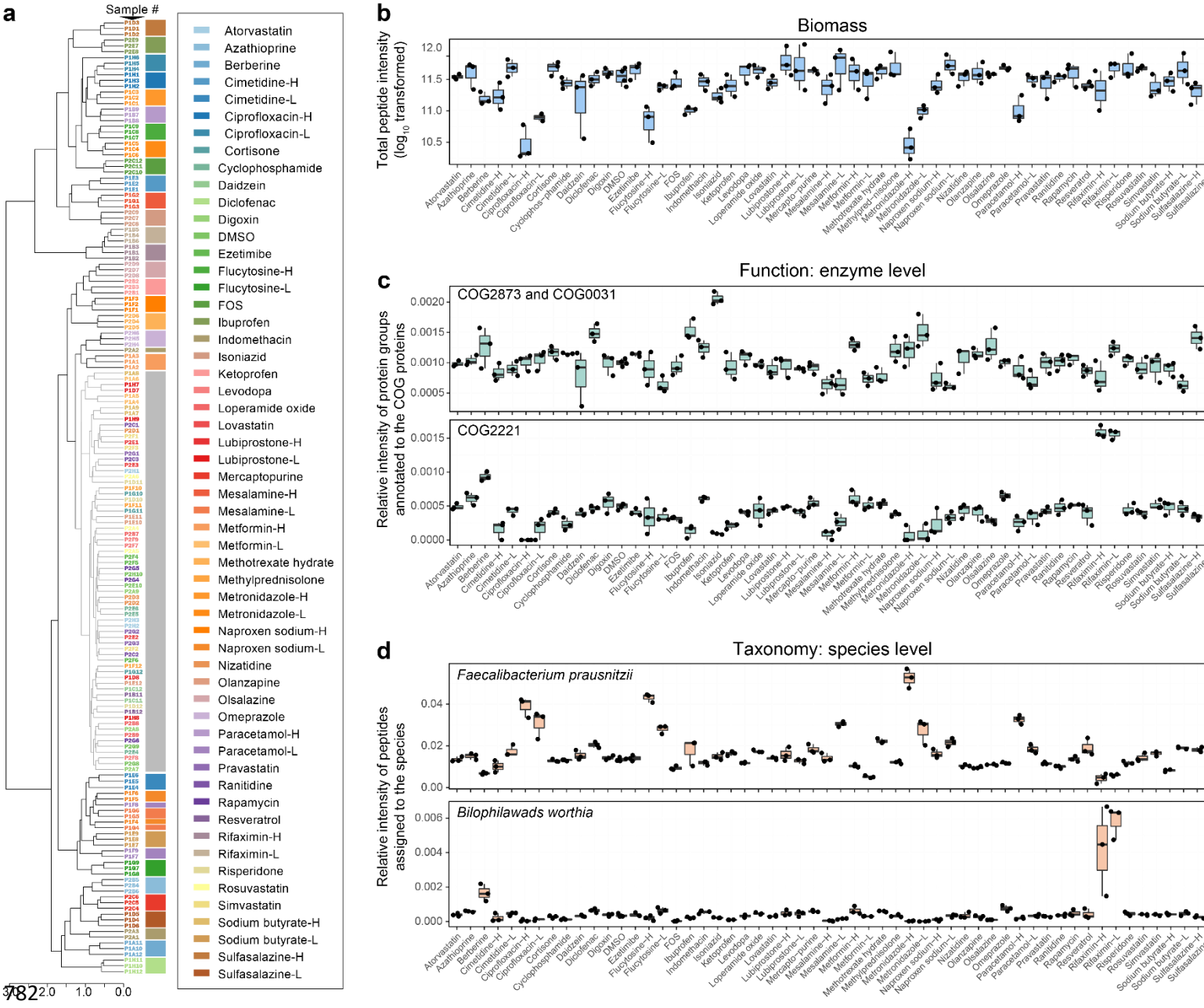

Figure S3. Reproducibility of RapidAIM assay on different levels.

(**a**) Clustering using protein group composition information showed that triplicates of drug treatments were closely clustered. A hierarchical tree was generated based on Pearson's correlation coefficient. The cluster corresponding to the gray box contained DMSO control samples; samples in this cluster indicated drugs that had very weak effects on the microbiome. (**b**) Box chart suggesting that biomass effects by drugs are highly reproducible. (**c**) Examples showing reproducible functional responses to drugs at the enzyme level. COC0031 and COG2873 are cysteine synthase and O-acetylhomoserine/O-acetylserine

sulfhydrylase (pyridoxal phosphate-dependent), respectively; both enzymes are involved in the conversion of sulfide to L-cysteine. [8] COG2221 is dissimilatory sulfite reductase (desulfoviridin), alpha and beta subunits; this enzyme reduces sulfite to sulfide [9]. (**d**) Examples showing reproducible taxonomic responses to drugs at the species level. *F. prausnitzii* is a ubiquitous bacterium of the intestinal microbiota [10]; *B. worthia* is a taurine-degrading bacterium which can reduce sulfite to sulfide by dissimilatory sulfite reductase [9]. COG2221 and *B. worthia* show a correlation in their response to different drugs. Box spans interquartile range (25th to 75th percentile), and line within box denotes median.

Supplementary Figure S4

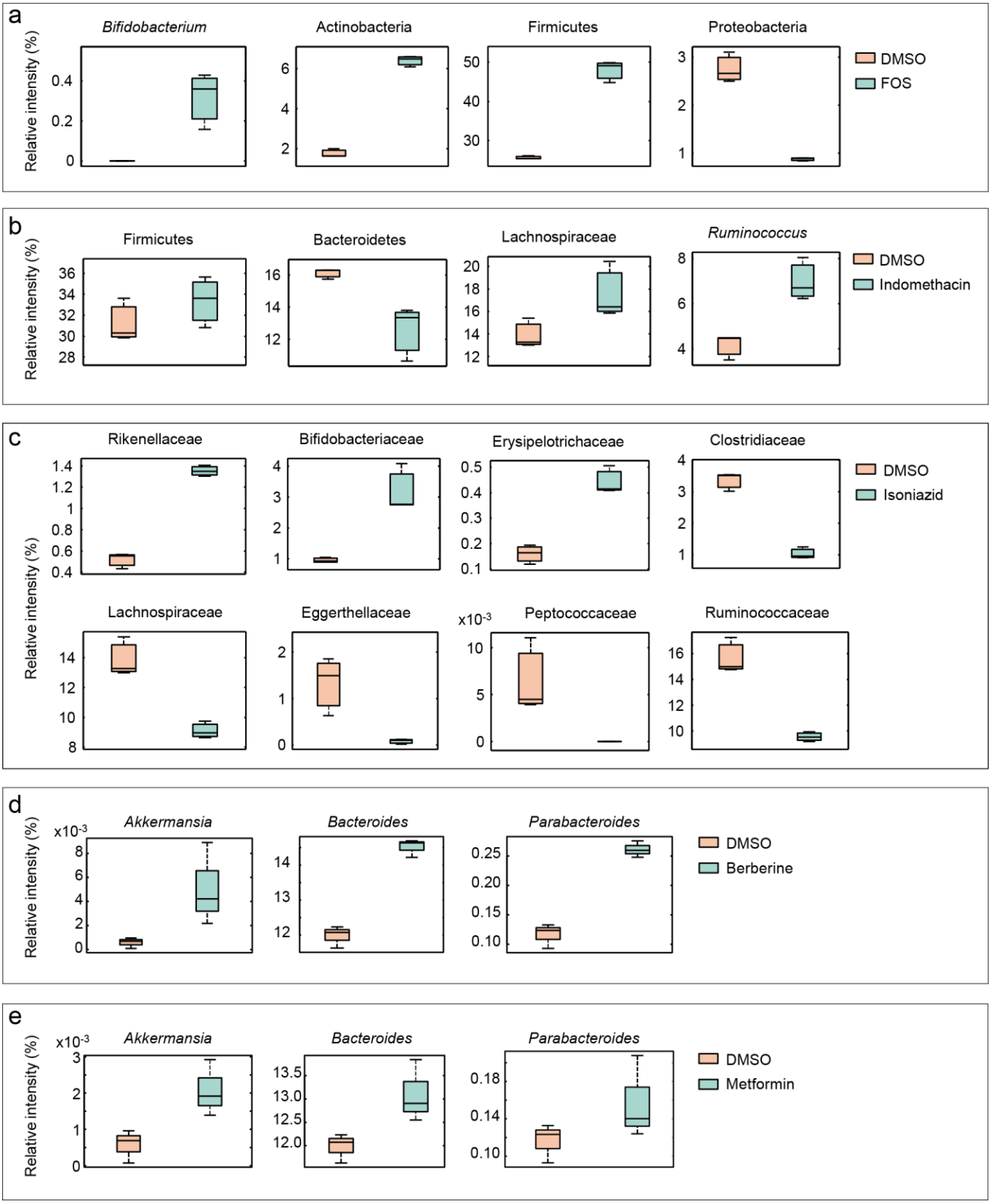

Figure S4. *In vitro* taxonomic responses to drugs reported in *in vivo* studies

(**a**) Hustoft et al. [11] showed increases in *Bifidobacterium*, Bacteroides, Actinobacteria, *Faecalibacterium. prausnitzii* and Firmicutes, and a decrease in Proteobacteria following a 10-day FOS treatment. Our results showed agreement with the above changes. Among which, the change of *Bifidobacterium*, Actinobacteria, Firmicutes and Proteobacteria showed statistical significance (*t*-tests based on technical triplicates, n=3, $p < 0.05$). (**b**) Liang et al. [12] observed changes in the phylums Bacteroidetes and Firmicutes, the genus *Ruminococcus*, and the family Lachnospiraceae as well as S24-7 (family), rc4-4, and Anaeroplasma after indomethacin treatment. Of these, Bacteroidetes, Firmicutes, genus *Ruminococcus*, and family Lachnospiraceae existed in our dataset. These taxa showed agreement with the above change. (**c**) Namasivayam et al. [13] reported alterations of 24 bacterial families in the microbiome of a mouse model of tuberculosis in response to a therapy containing isoniazid. In our dataset, 19 of those 24 families were found, and 15 (78.9 %) showed a trend for a similar response to isoniazid; 8 of these reached statistical significance ($p < 0.05$) in our results. (**d-e**) Others have reported increases of Akkermansia, Bacteroides and Parabacteroides in response to berberine [14,15] and metformin [16,17]. These increases were also found in our study. Box spans interquartile range (25th to 75th percentile), and line within box denotes median.

Supplementary Figure S5

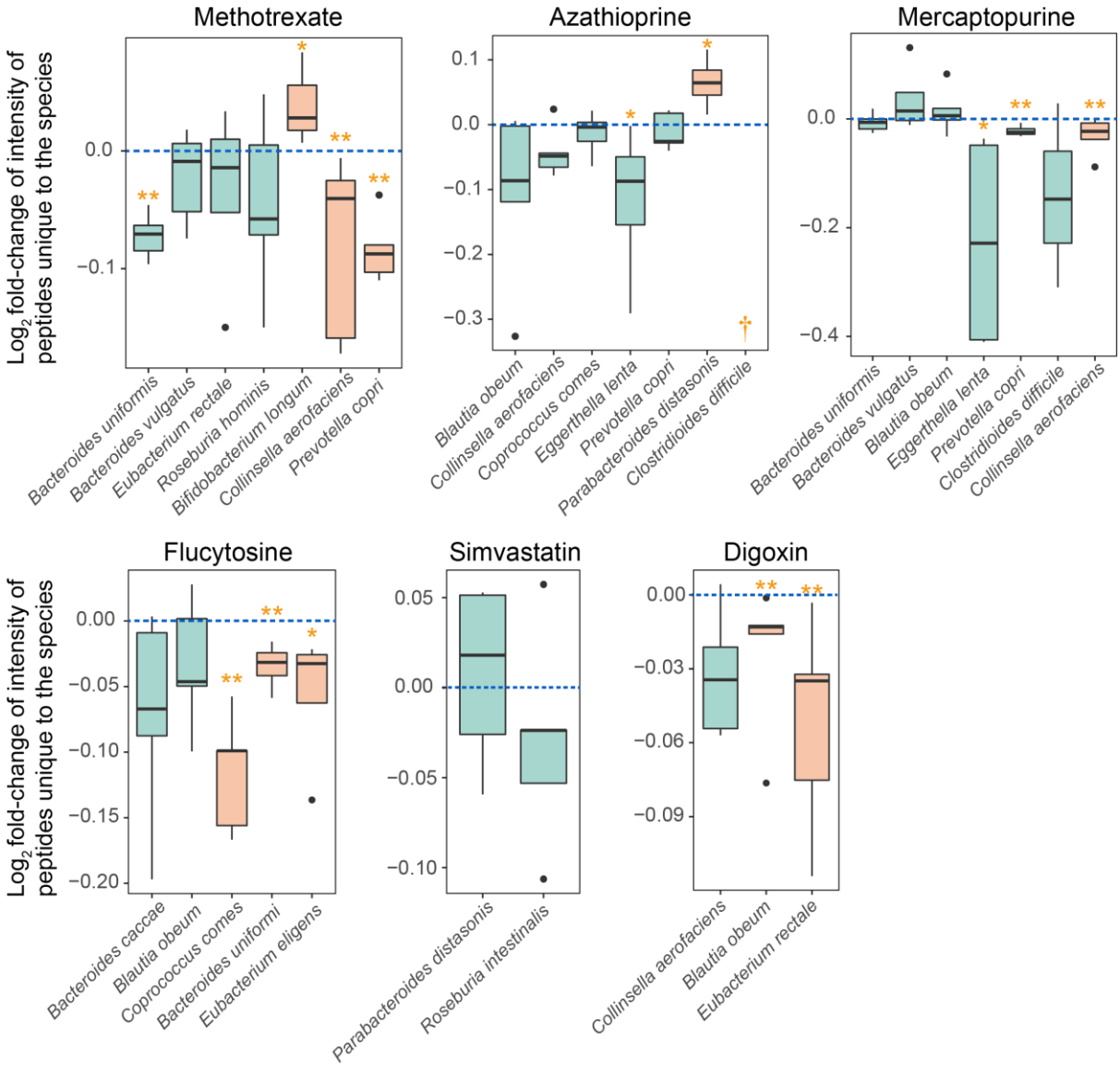

Figure S5. Comparison of species responses between RapidAIM POC and a pure culture-based study [18]

Thirty of our compounds (including 3 antibiotics) tested in the RapidAIM proof of concept study had been previously tested for their effect on single bacterial strain cultures [18]. Besides the 3 antibiotics, 6 of these compounds had an antibiotic-like effect in the single bacterial strain study. Blue boxes show the bacteria that were significantly inhibited in the single strain-based [18] studies, and the orange boxes represent other significant changes observed in our dataset. Orange stars showed the level of statistical significance in our study, which was evaluated by Wilcoxon rank sum test, FDR-adjusted *p*-values: *, $p < 0.05$; **, $p < 0.01$. † indicates that *C. difficile* was not detected in all samples after

azathioprine treatment. Box spans interquartile range (25th to 75th percentile), and line within box denotes median.

Supplementary Figure S6

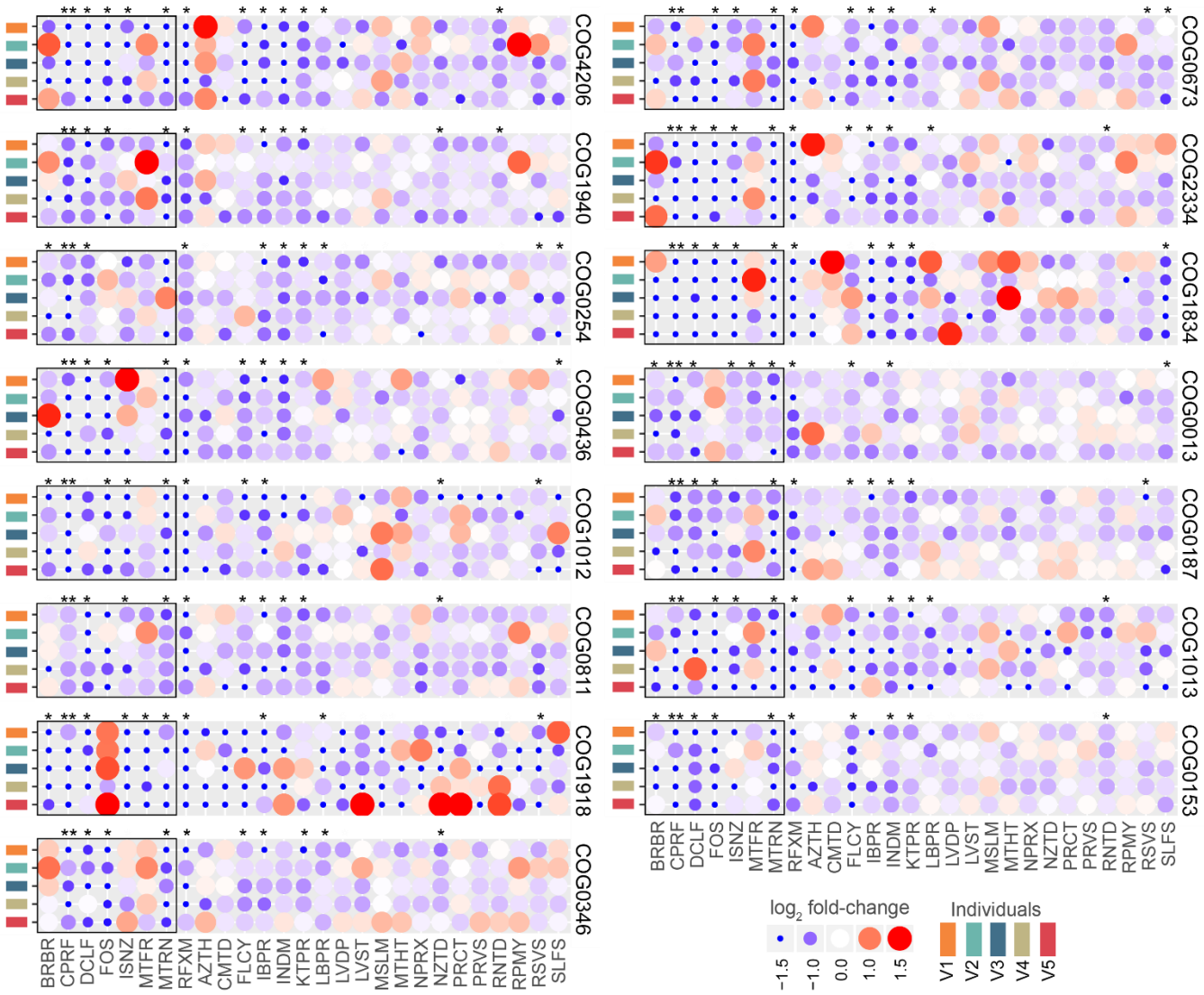

Figure S6. Log_2 fold-change of functions at the COG protein level

On the COG functional protein level, 535 COGs were significantly decreased by at least one drug treatment. The 15 COGs that were affected by ⩾ 10 compounds are shown in this figure. Statistical significance was evaluated by one-sided Wilcoxon rank sum test, FDR-adjusted *p*-values: *, $p < 0.05$; **, $p < 0.01$.

Supplementary Figure S7

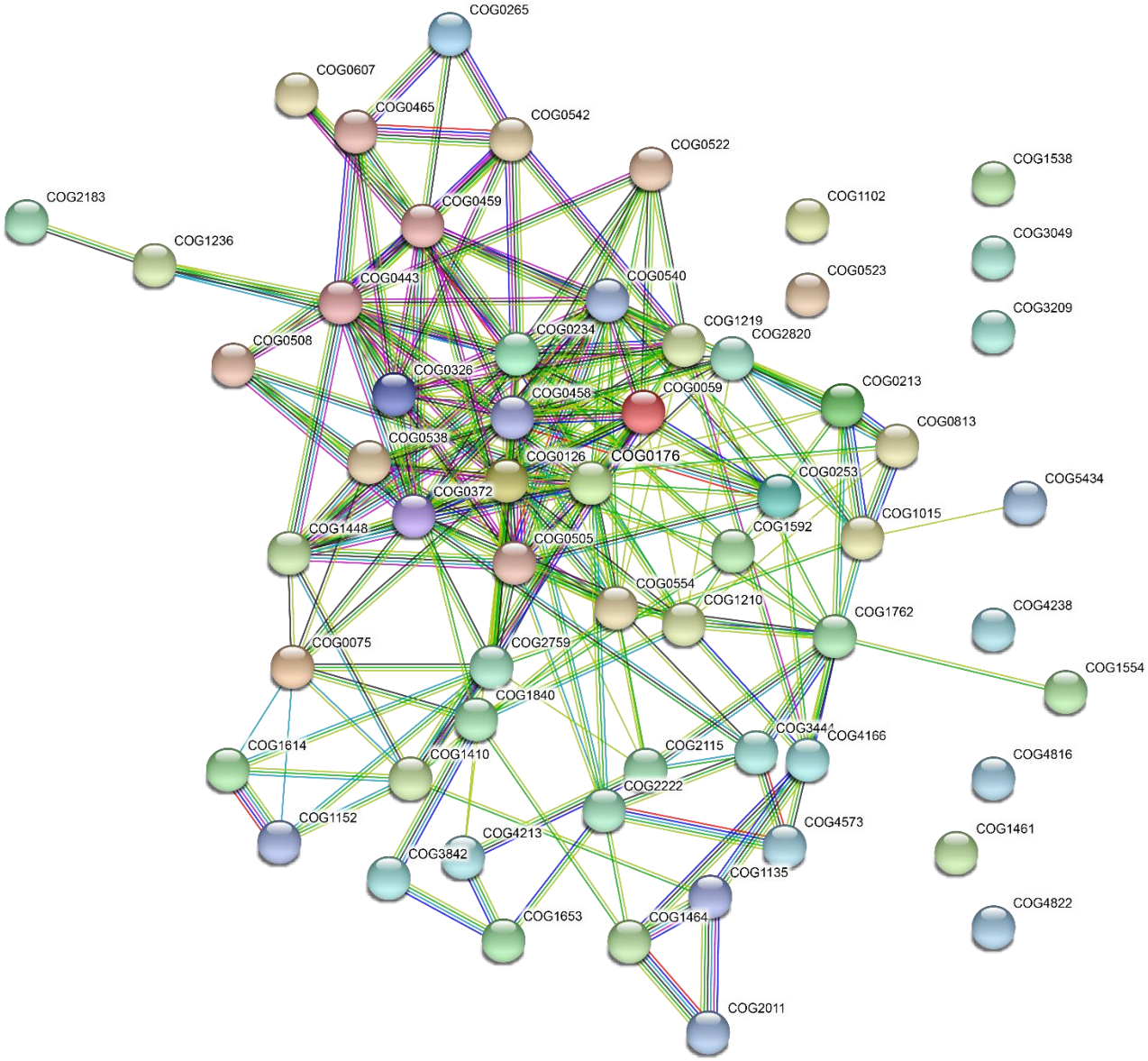

Figure S7. String interaction of COG functional proteins significantly stimulated by diclofenac

Supplementary Figure S8

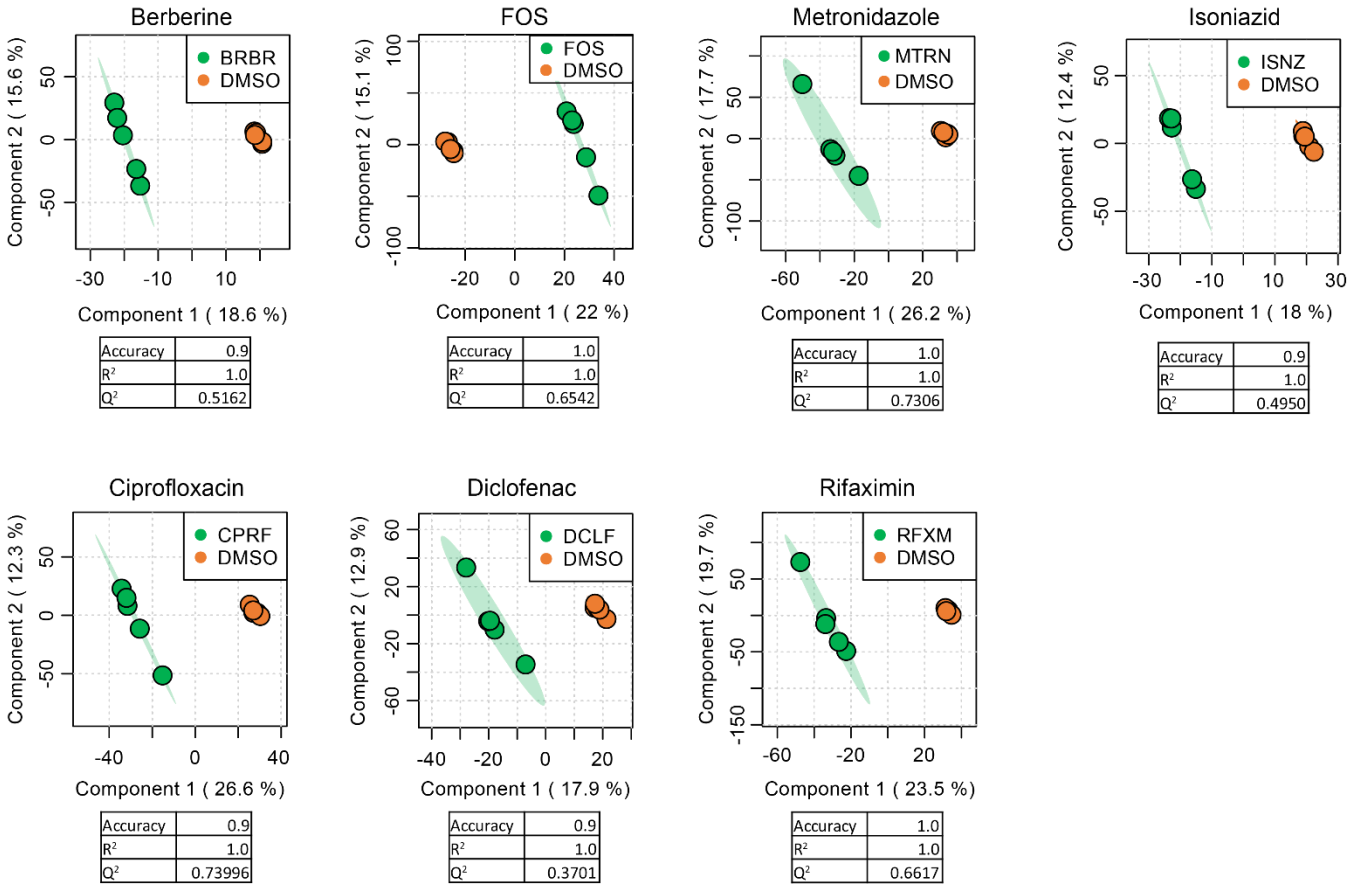

Figure S8. Score plots and cross-validations of seven PLS-DA models

PLS-DA models of microbiomes responses to each compound were established using MetaboAnalyst 4.0. PLS-DA model qualities were assessed through cross-validation, and accuracy, R^2 and Q^2 were given for each model. Seven compounds were found with valid PLS-DA models distinguishing the effect of the compound from the DMSO control.

Supplementary Figure S9

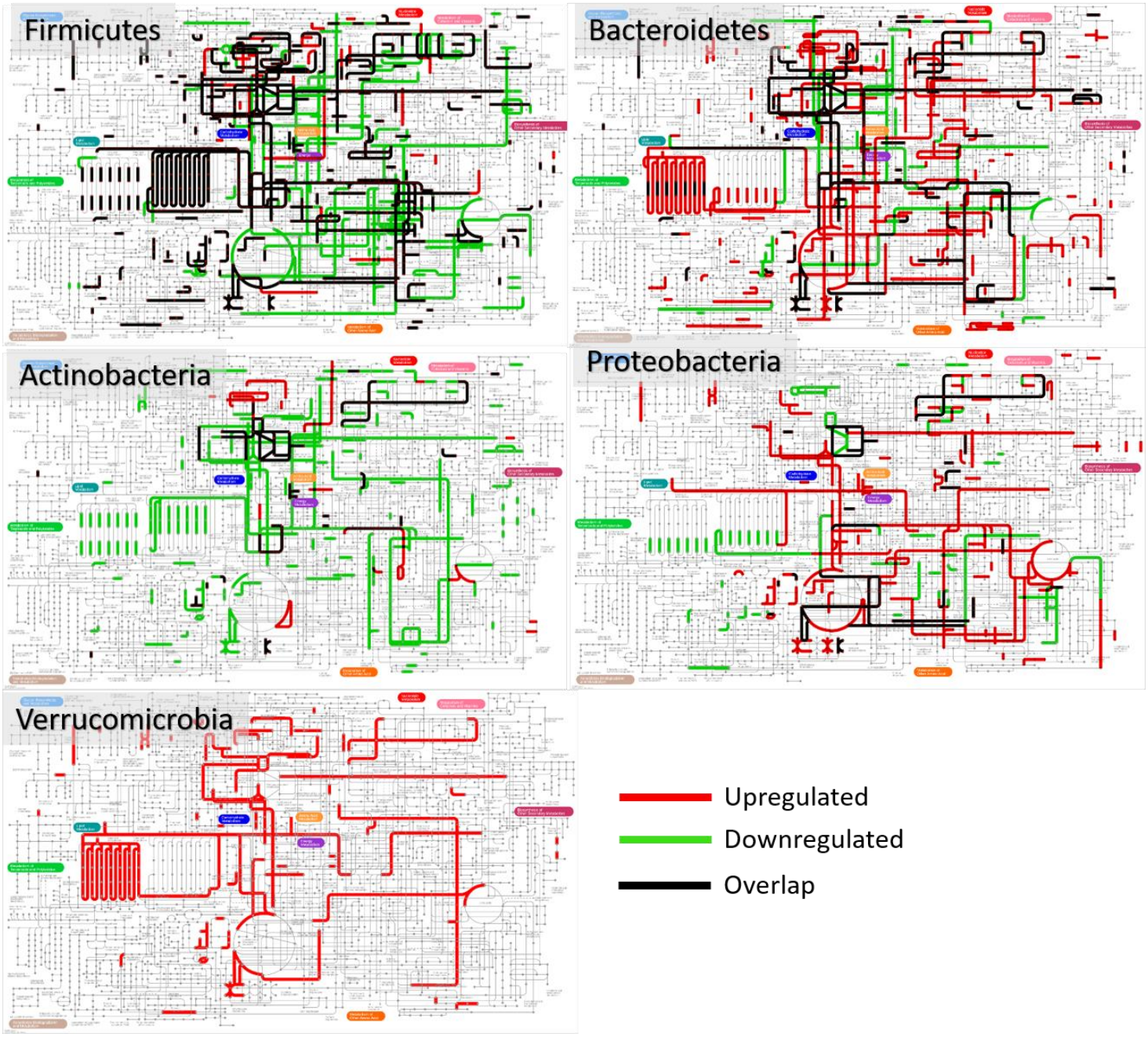

Figure S9. Phylum-specific functional responses to Berberine

Protein groups with VIP scores of >1 were annotated to phyla and COGs. Up- and down-regulated (red and green lines) COGs corresponding to different phyla were illustrated on a metabolic pathway map using iPath 3. Pathway maps for each phylum were combined, and overlapped pathways were shown in black lines. Our data suggest that different phyla responded differently at a functional pathway level.

Supplementary Figure S10

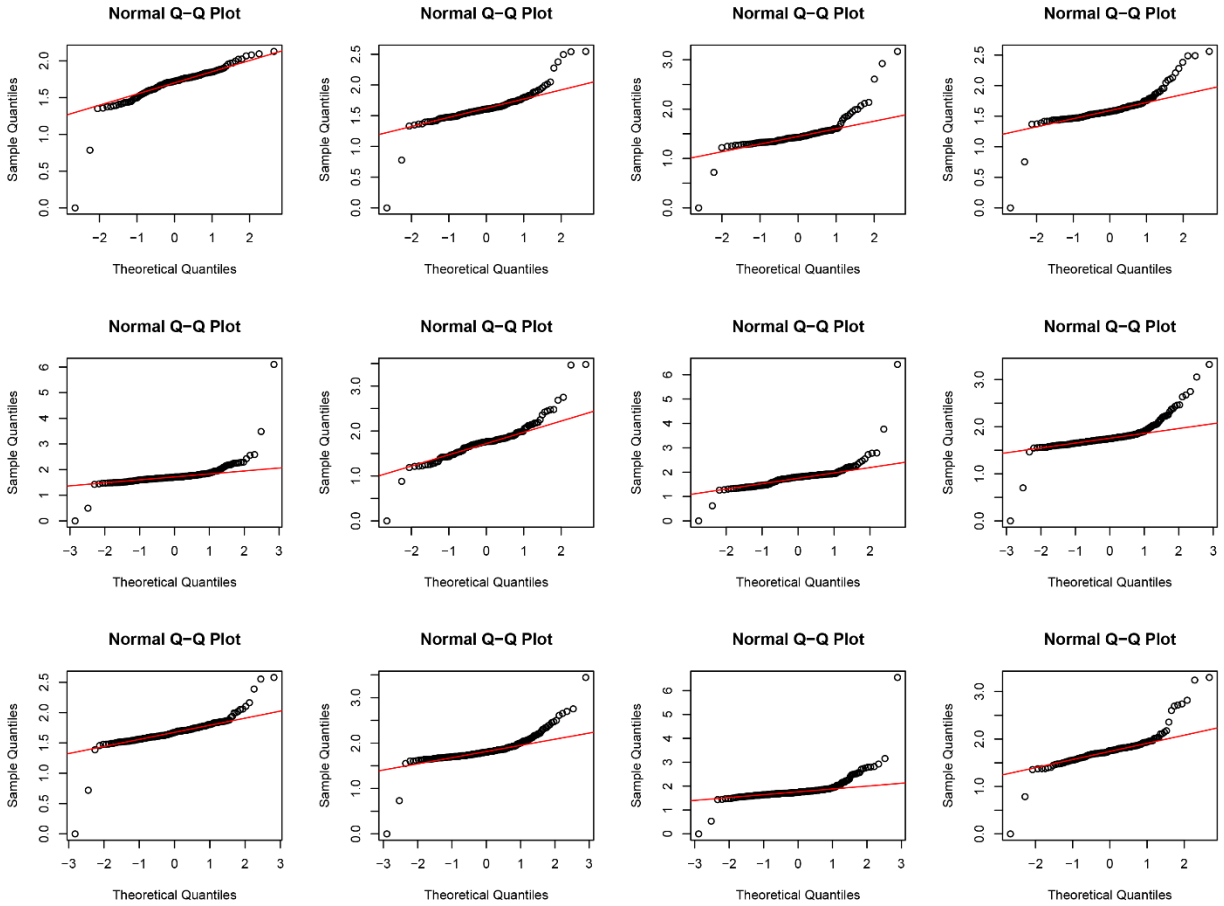

Figure S10. Randomly selected LFQ intensities of protein groups showing heavy tailed distribution on the Q-Q plots.

Supplementary Figure S11

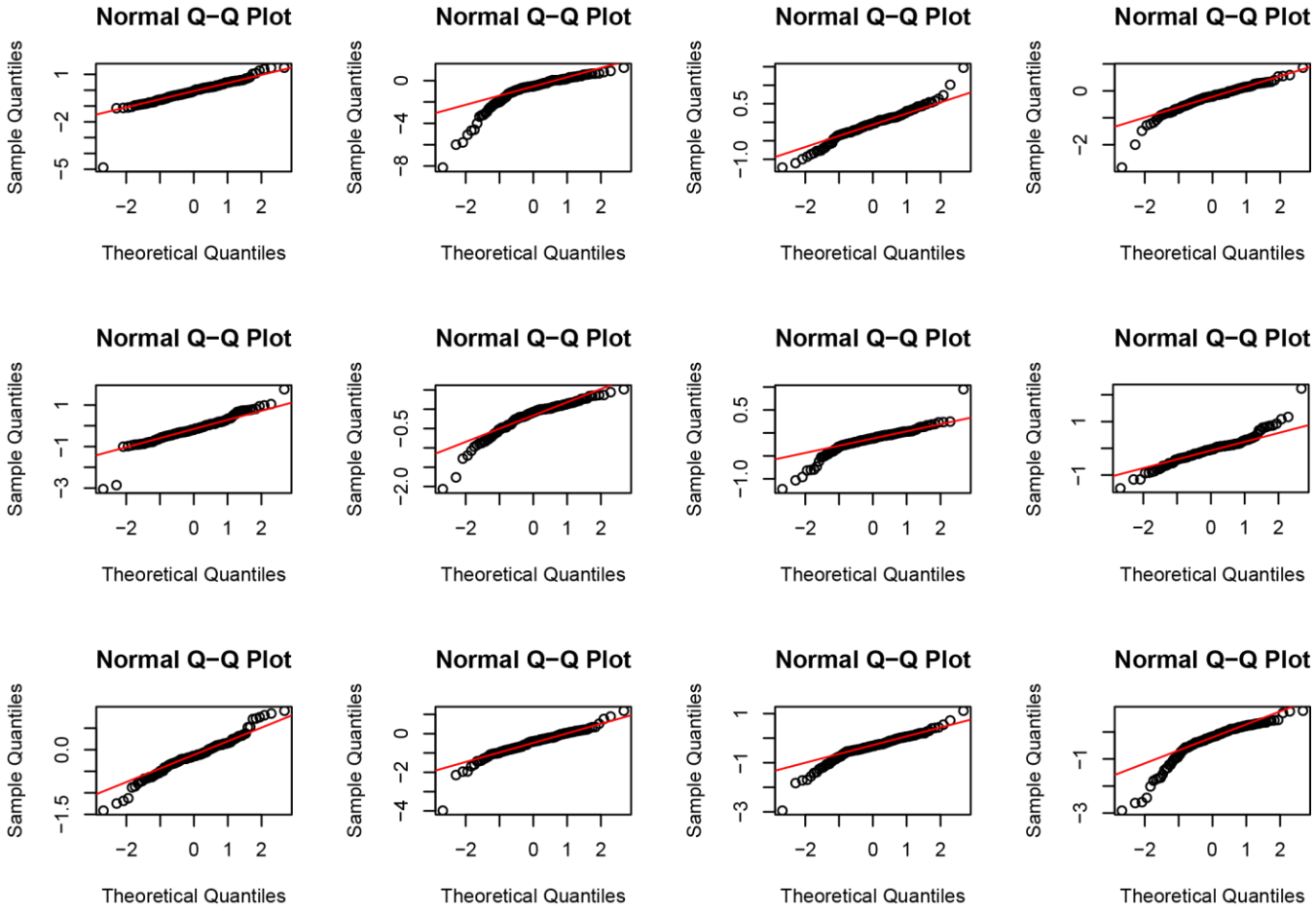

Figure S11. Randomly selected $\log_2$-fold changes of COGs showing heavy tailed distribution on the Q-Q plots.

References

1. Li, L.*, et al.* Evaluating in Vitro Culture Medium of Gut Microbiome with Orthogonal Experimental Design and a Metaproteomics Approach. *Journal of Proteome Research* **17**, 154-163 (2018).
2. Zhang, X.*, et al.* In Vitro Metabolic Labeling of Intestinal Microbiota for Quantitative Metaproteomics. *Analytical Chemistry* **88**, 6120-6125 (2016).
3. Zhang, X.*, et al.* Assessing the impact of protein extraction methods for human gut metaproteomics. *Journal of Proteomics* **180**, 120-127 (2018).
4. Defeu Soufo, H.J., Reimold, C., Breddermann, H., Mannherz, H.G. & Graumann, P.L. Translation Elongation Factor EF-Tu Modulates Filament Formation of Actin-Like MreB Protein In Vitro. *Journal of Molecular Biology* **427**, 1715-1727 (2015).
5. Mayer, F. Cytoskeletal Elements in Bacteria Mycoplasma pneumoniae, Thermoanaerobacterium sp., and Escherichia coli as Revealed by Electron Microscopy. *Journal of Molecular Microbiology and Biotechnology* **11**, 228-243 (2006).
6. Vértessy, B.G., Orosz, F., Kovács, J. & Ovádi, J. Alternative Binding of Two Sequential Glycolytic Enzymes to Microtubules: MOLECULAR STUDIES IN THE PHOSPHOFRUCTOKINASE/ALDOLASE/MICROTUBULE SYSTEM. *Journal of Biological Chemistry* **272**, 25542-25546 (1997).
7. Mayer, F. Cytoskeletons in prokaryotes. *Cell Biology International* **27**, 429-438 (2013).
8. Lithgow, J.K., Hayhurst, E.J., Cohen, G., Aharonowitz, Y. & Foster, S.J. Role of a Cysteine Synthase in Staphylococcus aureus</em&gt. *Journal of Bacteriology* **186**, 1579 (2004).
9. Laue, H., Friedrich, M., Ruff, J. & Cook, A.M. Dissimilatory Sulfite Reductase (Desulfoviridin) of the Taurine-Degrading, Non-Sulfate-Reducing Bacterium Bilophila wadsworthia RZATAU Contains a Fused DsrB-DsrD Subunit. *Journal of Bacteriology* **183**, 1727 (2001).
10. Miquel, S.*, et al.* Faecalibacterium prausnitzii and human intestinal health. *Current Opinion in Microbiology* **16**, 255-261 (2013).
11. Hustoft, T.N.*, et al.* Effects of varying dietary content of fermentable short-chain carbohydrates on symptoms, fecal microenvironment, and cytokine profiles in patients with irritable bowel syndrome. *Neurogastroenterology & Motility* **29**, e12969 (2016).
12. Liang, X.*, et al.* Bidirectional interactions between indomethacin and the murine intestinal microbiota. *eLife* **4**, e08973 (2015).
13. Namasivayam, S.*, et al.* Longitudinal profiling reveals a persistent intestinal dysbiosis triggered by conventional anti-tuberculosis therapy. *Microbiome* **5**, 71 (2017).
14. Zhu, L.*, et al.* Berberine treatment increases Akkermansia in the gut and improves high-fat diet-induced atherosclerosis in Apoe−/− mice. *Atherosclerosis* **268**, 117-126 (2018).
15. Zhang, X.*, et al.* Structural Changes of Gut Microbiota during Berberine-Mediated Prevention of Obesity and Insulin Resistance in High-Fat Diet-Fed Rats. *PLOS ONE* **7**, e42529 (2012).
16. Shin, N.-R.*, et al.* An increase in the Akkermansia spp. population induced by metformin treatment improves glucose homeostasis in diet-induced obese mice. *Gut* (2013).
17. Lee, H.*, et al.* Modulation of the gut microbiota by metformin improves metabolic profiles in aged obese mice. *Gut Microbes* **9**, 155-165 (2018).
18. Maier, L.*, et al.* Extensive impact of non-antibiotic drugs on human gut bacteria. *Nature* **555**, 623 (2018).